LEVEL

DTIC
APR 7 1980
S
C

A.R.A.P.

AERONAUTICAL RESEARCH ASSOCIATES *of* PRINCETON, INC.

80 3 19 011

A.R.A.P. REPORT NO 413

AKHP—

(14)

(6) VISCOUS THIN AIRFOIL THEORY

(10) John E. Yates

DTIC
ELECT
S APR 7 1980
D
C

Aeronautical Research Associates of Princeton, Inc.
50 Washington Road, P.O. Box 2229
Princeton, New Jersey 08540

(11)

(12) 65

February 1980

(9) Final Report. 1977—1980,

Prepared for

Office of Naval Research

under

Contract No. N00014-77-C-0616,

NAS1—15936

008400

Preface:

The work summarized in this final report was carried out over a three year period under Contract No. N00014-77-C-0616 to the Office of Naval Research. The technical monitor for the Navy was Mr. Mort Cooper. The final six months phase of the research effort was in part supported by NASA Langley Research Center under Contract No. NAS1-15936. The technical monitor for NASA was Dr. Carson Yates.

The assistance of Mr. Dave Dashcund in carrying out the numerical calculations is most gratefully acknowledged.

ABSTRACT

The theory of oscillating thin arifoils in incompressible viscous flow is formulated (see Refs. 1, 2, 3 for earlier background material) and applied to the calculation of steady and unsteady loads on the family of symmetric Joukowski airfoils. The theory is reduced to the form of an integral equation with kernel function whose solution is obtained with a modal expansion technique familiar from flat plate thin airfoil theory. The effect of viscosity is to change the order of the singularity in the kernel function such that a unique solution is obtained for any cross sectional geometry without using an auxilliary uniqueness criteria like the Kutta condition or principle of minimum singularity. The principal unsteady effect related to thickness is to introduce an explicit phase factor in the kernel function that is proportional to the time for vortex disturbances to be convected from the load point to the upwash point.

Viscous thin airfoil calculations for an airfoil with sharp trailing edge are in agreement with the results of potential theory with Kutta condition. The overall steady loads calculated with either theory are in general much larger than measured values and have the wrong trend with increasing thickness ratio. The competing effects of thickness (both geometric and boundary layer displacement) and viscosity for an actual airfoil are such that the measured loads are in better agreement with flat plate theory than with the theoretical results for finite thickness airfoils with sharp trailing edges.

Viscous thin airfoil steady and unsteady calculations for an airfoil with elliptic cross section are in much better agreement with experimental results. The slope of the steady state lift curve decreases with increasing thickness ratio in agreement with the experimental trend. The out of phase loads calculated for an oscillating elliptic section are significantly different from either flat plate results or those for the Joukowski airfoil with sharp trailing edge. The magnitude of the difference is in quantitative agreement with the differences between calculations based on Poisso's integral equation and recent experimental data.

It is concluded that viscous thin airfoil theory is a practical tool for introducing simultaneously the effects of viscosity and geometric thickness in two-dimensional unsteady aerodynamic theory.

i

CONTENTS

NOMENCLATURE

A_n coefficients in Chebyshev expansion of the load distribution, see Eq. (3.7)

a reference length, radius of circle corresponding to the Joukowski airfoils (quarter chord for flat plate airfoil)

a, b see Eq. (3.18)

C_{L_α} slope of the lift coefficient versus α curve at zero lift

C_{M_α} slope of the leading edge moment coefficient versus α curve at zero moment

C_{mn} see Eqs. (3.9) and (3.12)

C_o denotes modified airfoil surface, see Fig. 2.1

Cp_o surface pressure coefficient on non-lifting airfoil, see Eq. (2.2)

c airfoil chord

$\dfrac{D_\infty}{Dx}$ $v_\infty \dfrac{\partial}{\partial x} + i\omega$

$\exp(z)$ exponential function

$F(w)$ complex mapping of circle to Joukowski airfoil in the z-plane and flat plate in the Φ_o-plane, see Eqs. (3.13) and (3.14)

f perturbation displacement normal to airfoil surface

ε_m see Eq. (3.10)

h_o enthalpy field, non-lifting airfoil

h' perturbation enthalpy field

$h(x)$ airfoil thickness distribution

$K(\phi_o; \phi_o')$ kernel function, see Eqs. (2.29), (2.34), and (2.47)

$K_o(z)$ modified Bessel function

$K_1(x; y)$ integrated kernel, see Eq. (3.3)

k	$\omega c / 2 v_\infty$, reduced frequency
$\tilde{k}$	$2 \omega a / v_\infty$, modified reduced frequency (reduces to k for flat plate)
$\ell n(z)$	natural logarithm
M	Mach number
$\vec{n}_0$	unit vector normal to C_0 , see Fig. 2.1
P	k'/q_0^2
P_0	pressure field for non-lifting airfoil
Q_0^2	q_0^2/v_∞^2
q_0	surface speed on non-lifting airfoil
Re	$\dfrac{v_\infty c}{\nu}$ Reynolds number based on full chord
s	distance along airfoil surface
T	see Eq. (2.30) .
$T_n(x)$	Chebyshev polynomial of the first kind, Ref. 25, p. 774
t	time
$\vec{t}_0$	unit vector tangent to C_0 , see Fig. 2.1
$U_m(x)$	Chebyshev polynomial of the second kind, Ref. 25, p. 774
u_0, v_0	velocity components of non-lifting flow, see Eq. (2.19)
$\vec{v}_0$	velocity field for non-lifting airfoil
$\vec{v}'$	perturbation velocity field
v_∞	free stream velocity
$W(x,t)$	$\dfrac{D_0 f}{Dt}$, surface upwash
x	$\phi_0 / 2a \, v_\infty$ (Section III)
x_A, x_B	Cartesian coordinates of leading and trailing edge of flat plate airfoil

iv

x, y   Cartesian coordinates, see Fig. 2.1

$\mathscr{L}$ ΔP , see Eq. (2.23)

$\mathscr{R}$ see Eq. (2.26)

$\mathscr{W}$ $W/q_0 \quad = \quad \dfrac{\partial f}{\partial s} + \dfrac{i\omega}{q_0} f$

α angle of attack

γ 0.57721, Euler's constant

ΔP see Eq. (2.22)

$\Delta \phi$ see Eq. (2.22)

ϵ eccentricity parameter in Joukowski mapping, see Eq. (3.14)

$\theta(x,y)$ see Eq. (3.21) and Fig. 3.2

μ dynamic viscosity, $\rho_\infty \nu$

ν kinematic viscosity

ν^* see Eq. (2.35)

ρ_∞ fluid density

Σ see Eq. (3.18)

σ $v_\infty c/4\omega$, Reynolds number referred to quarter chord

$\tilde{\sigma}$ $v_\infty a/\nu$ (reduces to σ for flat plate)

τ true thickness to chord ratio

τ^* modified thickness ratio

τ_{ij} viscous stress of non-lifting flow

ϕ_0 potential of non-lifting flow

ϕ' perturbation potential

ϕ_A, ϕ_B value of ϕ_0 at leading and trailing edge of nonlifting airfoil

ψ_0	stream function of non-lifting flow
Ω'	perturbation vorticity
ω	radian frequency of simple harmonic motion

$\dfrac{D_0}{Dt}$	$\dfrac{\partial}{\partial t} + \vec{v}_0 \cdot \text{grad}$
div	divergence operator
grad	gradient operator
$|q|$	absolute value of quantity q
∇^2	Laplace operator

I. INTRODUCTION

The linearized inviscid potential theory of thin airfoils has served the unsteady aerodynamicist well for many years. In fact the rapid development of modern high speed aircraft following the second World War would have been severely impeded without this powerful theoretical tool. Today, each aircraft manufacturer has its own computational package for carrying out aeroelastic calculations that incorporates a vast array of accumulated theoretical and practical knowledge on the unsteady aerodynamic problem. When these computational methods are used by the experienced aerodynamicist and with a certain amount of empirical "tailoring" of the unsteady loads, reasonably good agreement with experimental measurements can be obtained. Unfortunately, the most commonly used practical index for comparison with experiment on actual aircraft has been the flutter or divergence speed of the wing - the end result of a rather elaborate aerodynamic and aeroelastic calculation. When theory and experiment do not agree there are many underlying assumptions, both physical and mathematical, that can be blamed, most of which focus on some aspect of the unsteady aerodynamic problem.

An obvious missing element in thin airfoil theory is the geometric shape of the airfoil section. If the flow is incompressible, inviscid and two-dimensional, the effect of geometric shape is in principle no problem. One can use the powerful techniques of conformal mapping to obtain an exact solution of the potential flow problem for an airfoil of any cross-sectional geometry that undergoes arbitrary unsteady motion. Unfortunately, there is a one parameter family of such solutions for unsteady or steady flow, all of which satisfy the boundary conditions of the potential flow problem. The uniqueness problem is even more acute for the three-dimensional problem, since the spanwise "distribution" of the circulation can be specified arbitrarily. For the two- or three-dimensional potential flow problem the important point is that some auxilliary condition must be specified to obtain a unique solution. In the usual application of potential flow theory it is customary to apply the Kutta condition at the trailing edge of the airfoil.

The validity of the Kutta condition in unsteady aerodynamics application has been seriously questioned and debated in the literature (e.g., see Refs. 10, 11, 12). It is generally recognized that the conventional thin airfoil theory is at best unreliable when applied to hydrofoil flutter problems where the reduced frequency is of order unity or greater (Refs. 13, 14, 15, 16). The "smooth" flow at the trailing edge that is observed in steady flow is expected to break down at some reduced frequency. In recent experimental work (Ref. 10) measurements

1

have been made of the surface pressure distribution very close to the trailing edge. It was found that locally large departures from potential flow behavior can occur even for moderately low reduced frequencies.

The local breakdown of the potential flow near the trailing edge of an oscillating or fixed airfoil should not be surprising. If potential theory is interpreted as a model of the real flow including the boundary layer and wake then we can safely argue that potential theory is at its very "worst" in the vicinity of the trailing edge. Yet that is precisely where all of the emphasis is placed in the usual application of a uniqueness criterion like the Kutta condition. Experimentally, there is no question that the surface pressure near the trailing edge of a lifting airfoil in steady flow is not only finite but almost fully recovered to the non-lifting value. However, if the "absence of a trailing edge pressure singularity" is used as a uniqueness criterion with potential theory the lift distribution over the entire airfoil will be overpredicted and the lift curve can easily be 25% too large. Also the theoretical lift curve slope increases, in proportion to the thickness ratio while the experimental values are usually constant or decrease with increasing thickness (see Fig. 3.5, p. 39).

It was shown by Pinkerton (Ref. 17) that if the measured lift is used to determine the unknown circulation in potential theory, then the theoretical and experimental pressure distributions are in reasonably good agreement (see Fig. 1.1) over the forward 95% of the airfoil. Furthermore, when the airfoil shape was modified slightly (including a small trailing edge bluntness) to account for boundary layer displacement effects, Pinkerton obtained near perfect agreement between theory and experiment even to the extent of eliminating the trailing edge singularity. At this point it should be emphasized that the only reason potential theory has a singularity in the first place is because the trailing edge is mathematically sharp. It is only for a sharp trailing edge that the Kutta condition can be stated in a mathematically precise way and in general it leads to serious errors even for that special geometry.

The important conclusion from Pinkerton's work is that for "well designed" high Reynolds number airfoils (i.e., no separation over the forward part of the airfoil), inviscid potential flow theory, including geometric and boundary layer displacement effect is completely adequate to calculate the detailed pressure distribution. The only stipulation is that one must give up the Kutta condition or any other uniqueness criteria that overemphasizes the detailed behavior of the local trailing edge flow. The "fundamental question" of potential
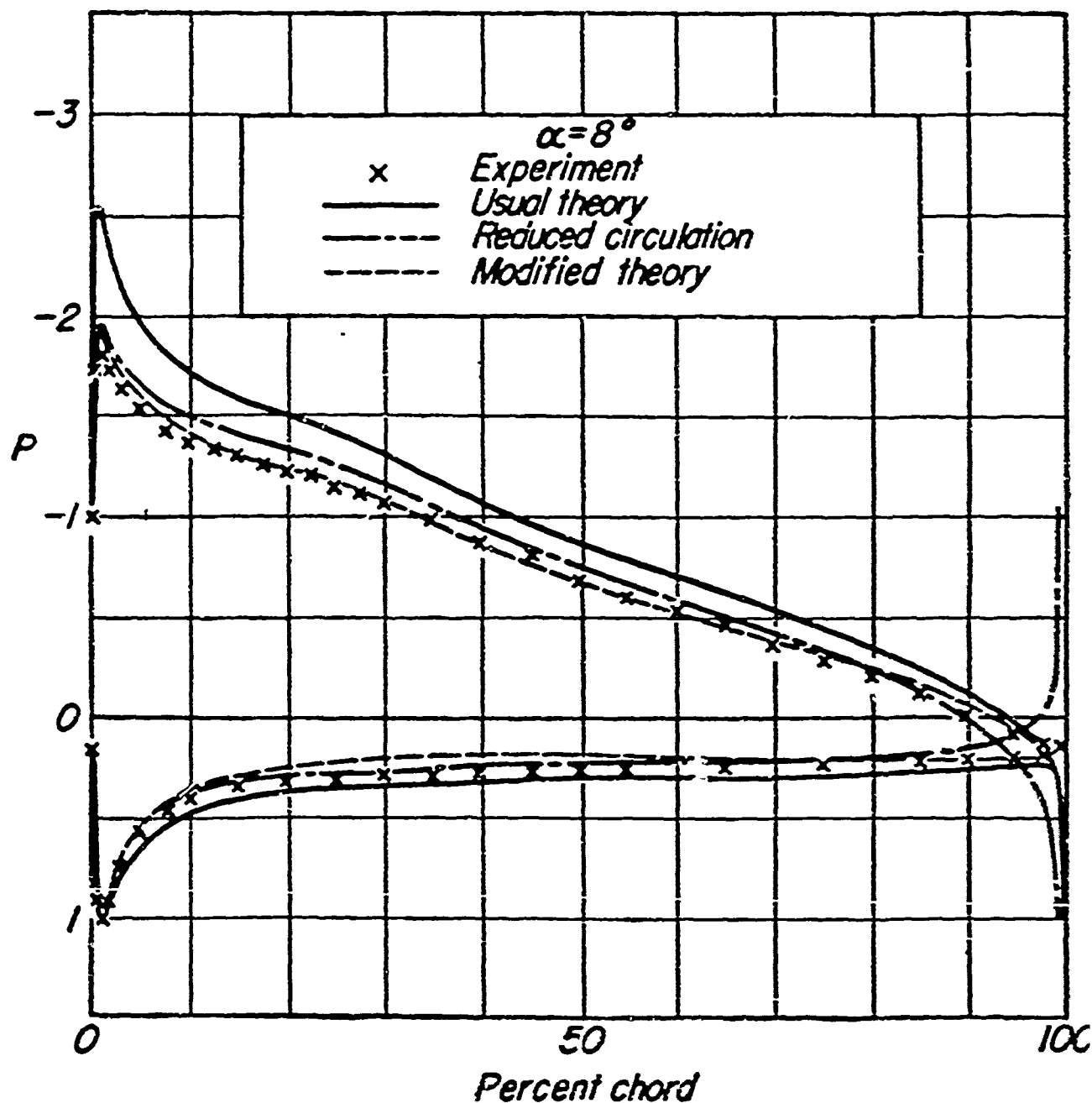
2

Figure 1.1. – Comparison between measured and various theoretical pressure distributions on a NACA 4412 wing section due to Pinkerton (Ref. 17, p. 62).

flow theory still remains; i.e., how can we calculate the unknown circulation? For the unsteady aerodynamicist, the question is particularly important since experimental measurements of the unsteady sectional circulation are seldom available.

The answer to the "fundamental question" of potential theory must ultimately be found by consideration of the direct effect of viscosity, the most important missing physical element of conventional thin airfoil theory. It follows from the d'Alembert paradox (see Ref. 18, p. 322 and 405) that the origin of any net force on a finite body in an unbounded flow must be due to viscous effects no matter how large the Reynolds number. The expression "inviscid potential theory of lift" is a misnomer. One must evaluate the lift in the limit as the Reynolds number tends to very large values, a point that was emphasized in a recent paper of Sears (Ref. 19). The Kutta condition itself is a statement about the direct effect of viscosity although the student of aerodynamics rarely gets more than a brief heuristic physical argument to justify its origin.

It was shown theoretically by Shen and Crimi (Ref. 20) and by direct calculation in the present report that the Kutta condition is the correct viscous uniqueness criterion in the high Reynolds number limit for airfoils with a mathematically sharp trailing edge. The proof of uniqueness of the thin airfoil problem using Oseen's theory as in Ref. 20, or viscous thin airfoil theory as in this report, should be included in any modern text book or college level course on the theory of lift. The flat plate theory (see Section II.C) is straight-forward and permits one to see the explicit connection between the effect of viscosity in the Stokes layer and the lift on an airfoil.

The practical limitation of the flat plate theory is that direct viscous effects are "grossly" overexaggerated because of the mathematically sharp trailing edge. Recall from Pinkerton's work (Ref. 17) that the same criticism can be leveled at the Kutta condition (also see Section III.C). The trailing edge Reynolds number (i.e., based on the edge thickness) of typical airfoils is of the order of 10^3 or 10^4. If the Reynolds number is based on the displacement thickness at the trailing edge the numbers are more like 10^4 or 10^5. The geometric edge is totally immersed in a turbulent shear flow and the direct effect of viscosity near the trailing edge is diminished. The details of the trailing edge flow practically defy analysis and serious attempts to analyze the problem have been restricted to airfoils with sharp trailing edges (see Refs. 21, 22, 23). It is a basic premise of the present author that the ultra-detail of the trailing edge flow cannot be of serious practical

4

importance to the unsteady aerodynamicist. The arguments to support this claim are based on a mixture of experimental and theoretical evidence. First of all the overall lift and moment (and higher order moments required for aeroelastic analysis) of an airfoil at high Reynolds number ($> 10^6$) are "linear" functions of the angle of attack. The trailing edge flow is very nonlinear (separated and turbulent) and yet the nonlinearity does not appear in the overall loads until the stall speed is approached. On the other hand, a nonlinear leading edge flow has a profound nonlinear effect on the overall loads (see Section III.C, Fig. 3.7).
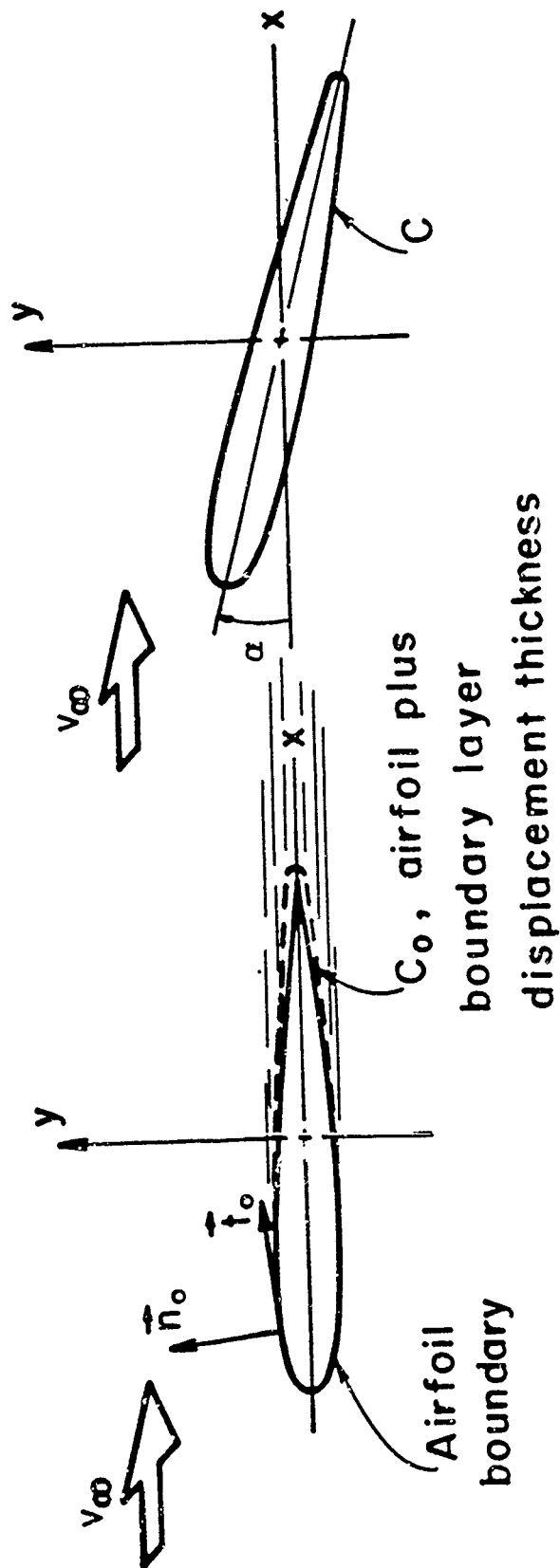
Other evidence to support our claim of "trailing edge independence" may be inferred from the recent unsteady airfoil experiments of Davis and Malcolm (Ref. 24). All of their unsteady surface pressure measurements exhibit a linear simple harmonic relation to the forced motion of the airfoil. No second harmonic content of any magnitude was detected in the measurements. Also, the measured unsteady loads are virtually zero over the aft 10% of the chord for reduced frequencies up to 0.3. Therefore, the trailing edge loads, whether they are linear or nonlinear, do not contribute to the overall load coefficients required in aeroelastic analyses.

The effect of viscosity at the trailing edge is de-emphasized in the present work by considering an effective trailing edge bluntness, thus eliminating the associated potential flow singularity as in the work of Pinkerton. The direct effect of viscosity over the entire geometric cross section corrected for boundary layer displacement is the physical origin of the circulatory lift. The calculation of the unsteady loads, including geometric and viscous effects, is the primary aim of viscous thin airfoil theory. The basic mathematical concepts are formulated in detail in Section II. An integral equation is derived that relates the loads and upwash via a kernel function that includes the essential effects of geometry and viscosity. Numerical calculations of the loads on fixed and oscillating airfoils of the Joukowski family are compared with experimental data in Section III.

II.   VISCOUS THIN AIRFOIL THEORY

A.   Basic Concepts and Equations

Consider a thin two-dimensional symmetric airfoil in an incompressible flow at zero angle of attack (Fig. 2.1a). For very high Reynolds number the nonlifting pressure distribution may be calculated quite accurately with potential flow theory (e.g., see Fig. 1.1). If the thin boundary layer displacement thickness is added to the geometric thickness (dashed line in

(a) Airfoil at zero angle of attack
with mean boundary layer

(b) Perturbed modified
airfoil shape

Figure 2.1. - Geometry of the viscous thin airfoil problem and removal of the
symmetric boundary layer.

6

Fig. 2.1a) even greater accuracy may be obtained. Alternatively, given the measured surface pressure distribution on an actual body, one can solve the inverse potential flow problem and determine the precise shape of a "modified body" that will induce such a pressure distribution. Except perhaps in the immediate vicinity of the trailing edge, the difference between the modified and actual body shapes will be of the order of the boundary layer displacement thickness.

The nonlifting potential flow so constructed, may be interpreted in a slightly different way. The modified airfoil in Fig. 2.1a may be thought of as a real airfoil whose upper and lower surfaces move at precisely the potential flow speed, q_0, calculated from the inverse Bernoulli relation

$$\frac{q_0^2}{v_\infty^2} = 1 - Cp_0 \tag{2.1}$$

with the surface pressure coefficient

$$Cp_0 = \frac{p_0 - p_\infty}{\frac{1}{2}\rho_\infty v_\infty^2} = \frac{h_0 - h_\infty}{\frac{1}{2}v_\infty^2} \tag{2.2}$$

The potential flow solution for the modified airfoil may then be interpreted as an exact viscous solution of the Navier-Stokes equations; i.e.,

$$\text{div}\,\vec{v}_0 = 0 \tag{2.3}$$

$$\vec{v}_0 \cdot \text{grad}\,\vec{v}_0 + \text{grad}\,h_0 = \nu \nabla^2 \vec{v}_0 \tag{2.4}$$

$$\left.\begin{aligned} \vec{n} \cdot \vec{v}_0 &= 0 \\ \vec{t} \cdot \vec{v}_0 &= q_0 \end{aligned}\right\} \quad \text{on } C_0 \tag{2.5}$$

$$\vec{v}_0 \sim \vec{v}_\infty \quad \text{at } \infty \tag{2.6}$$

The vorticity is zero everywhere so that

$$\vec{v}_0 = \text{grad } \phi_0 \qquad (2.7)$$

The viscous stress is given by the expression

$$\tau_{ij} = \mu \left(\frac{\partial v_0^i}{\partial x^j} + \frac{\partial v_0^j}{\partial x^i} \right) = 2\mu \frac{\partial^2 \phi_0}{\partial x^i \partial x^j} \qquad (2.8)$$

It is not zero but its divergence is zero so that $\vec{v}_0$, h_0 are also solutions of the inviscid Euler equations.

The purpose of the foregoing construction, is to remove the thin turbulent boundary layer and wake on the actual airfoil. The geometric airfoil shape has been modified slightly to account for the high Reynolds number boundary layer displacement thickness. We are left with an exact viscous-potential flow over a modified body C_0 with a moving surface and a surface pressure distribution that is as close to the actual measured pressure distribution as we choose to calculate. Finally, we emphasize the point that the constructed equivalent airfoil and potential flow will represent the actual airfoil and real flow "best" at high Reynolds number. It is tacitly assumed, of course, that the actual airfoil is "designed" for high Reynolds number operation with an attached boundary layer flow, except perhaps near the trailing edge.

We now pose the fundamental question of viscous thin airfoil theory. What load distribution is induced on the "modified" airfoil when it is perturbed from its nonlifting configuration? (See Fig. 2.1b.) The surface displacement and/or velocity is assumed to be small but may otherwise be steady or unsteady. The modified airfoil surface is assumed to undergo the same deformation as the actual airfoil surface; i.e., the boundary layer thickness is assumed to be "frozen". The perturbed flow (denoted by a primed variable) satisfies the following set of linearized viscous equations:

$$\text{div } \vec{v}' = 0 \qquad (2.9)$$

$$\frac{D_0 \vec{v}'}{Dt} + \vec{v}' \cdot \text{grad } \vec{v}_0 + \text{grad } h' = \nu \nabla^2 \vec{v}' \qquad (2.10)$$

where

8

$$\vec{v}' = \vec{v} - \vec{v}_o$$

$$h' = h - h_o \qquad (2.11)$$

and

$$\frac{D_o}{Dt} = \frac{\partial}{\partial t} + \vec{v}_o \cdot \text{grad} \qquad (2.12)$$

Also, $\vec{v}'$ must vanish at infinity and satisfy viscous boundary conditions on the modified airfoil surface; i.e.,

$$\vec{v} = \vec{v}_o + \vec{v}' = \vec{v}_o^s \qquad \text{on C} \qquad (2.13)$$

(see Fig. 2.1b), where $\vec{v}_o^s$ is the specified surface velocity. For the lifting problem we assume that the perturbation displacement and velocity are everywhere normal to the unperturbed surface, C_o. Then the projection of the boundary conditions onto C_o (see Fig. 2.1b) yields the following two conditions:

$$\vec{n}_o \cdot \vec{v}' = \frac{D_o f}{Dt} \qquad (2.14)$$

$$\left. \begin{array}{c} \\ \\ \end{array} \right\} \text{ on } C_o$$

$$\vec{t}_o \cdot \vec{v}' = 0 \qquad (2.15)$$

where f is the perturbation displacement normal to the unperturbed surface. The first boundary condition is recognized as the familiar inviscid requirement of no flow through the surface. The second condition is a "viscous" no-slip condition on the "perturbation flow". The fundamental problem of viscous thin airfoil theory is to solve Eqs. (2.9) and (2.10) in the limit as $\nu \to 0$, subject to the boundary conditions (2.14) and (2.15) and the requirement of a vanishing perturbation flow at infinity.

B. The Associated Potential Flow Problem

If the viscosity is set equal to zero in Eq. (2.10) and the viscous boundary condition Eq. (2.15) is dropped, we recover the familiar "inviscid" linearized potential flow problem for the load distribution. Introduce a perturbation

9

velocity potential such that

$$\vec{v}' = \text{grad } \phi' \tag{2.16}$$

then the "inviscid" problem becomes

$$\nabla^2 \phi' = 0$$

$$h' = - \frac{D_0 \phi'}{Dt}$$

$$\frac{\partial \phi'}{\partial n_0} = \frac{D_0 f}{Dt} = W(x,t) \qquad \text{on } C_0$$

$$|\vec{v}'| \sim 0 \qquad \text{at } \infty \tag{2.17}$$

In addition to the boundary conditions on the surface and at infinity, we must impose one additional and all important condition to obtain a unique solution of the potential flow problem. For the moment we leave this uniqueness condition open.

The potential flow problem can of course be solved exactly by conformal mapping techniques. Here we derive an integral equation from which we can subsequently formulate the viscous problem for a body with thickness. In the remainder of this report we assume that all perturbation variables have a simple harmonic time dependence; i.e.,

$$q(\vec{x},t) = q(\vec{x}) e^{i\omega t} \tag{2.18}$$

where ω is the radian frequency. Next we introduce a conformal coordinate transformation in Eqs. 2.17 that maps the airfoil onto a "slit" on the real axis. If ϕ_0, ψ_0 are the conjugate potential and streamfunction corresponding to the thickness induced flow field, i.e.,

$$u_0 = \frac{\partial \phi_0}{\partial x} = \frac{\partial \psi_0}{\partial y}$$

$$\tag{2.19}$$

$$v_0 = \frac{\partial \phi_0}{\partial y} = - \frac{\partial \psi_0}{\partial x}$$

10

then ϕ_0, ψ_0 are suitable mapping functions. In ϕ_0, ψ_0 coordinates the potential flow problem becomes (see Fig. 2.2)

$$\nabla^2 \phi' = \frac{\partial^2 \phi'}{\partial \phi_0^2} + \frac{\partial^2 \phi'}{\partial \psi_0^2} = 0$$

$$\left.\frac{\partial \phi'}{\partial \psi_0}\right|_{\psi_0 = 0^{\pm}} = W/q_0 = \mathcal{W} \qquad \phi_A < \phi_0 < \phi_B$$

$$\frac{\partial \phi'}{\partial \phi_0} + \frac{i\omega}{q_0^2} \phi' = -\frac{h'}{q_0^2} = -P \qquad\qquad (2.20)$$

$$|\text{grad } \phi'| \sim 0 \qquad \text{at } \infty \qquad\qquad (2.21)$$

Let

$$\Delta\phi = \phi'(\phi_0, 0^-) - \phi'(\phi_0, 0^+)$$

$$\Delta P = P(\phi_0, 0^-) - P(\phi_0, 0^+) = \frac{\Delta h'}{q_0^2} \qquad\qquad (2.22)$$

Then

$$\frac{\partial \Delta\phi}{\partial \phi_0} + \frac{i\omega}{q_0^2} \Delta\phi = -\Delta P \equiv -\mathcal{L}(\phi_0) \qquad\qquad (2.23)$$

and

$$\Delta\phi = -\int_{\phi_A}^{\phi_0} \mathcal{L}(\phi_0') \exp\left(-i\omega \int_{\phi_0'}^{\phi_0} \frac{d\phi_0''}{q_0^2}\right) d\phi_0' \qquad\qquad (2.24)$$

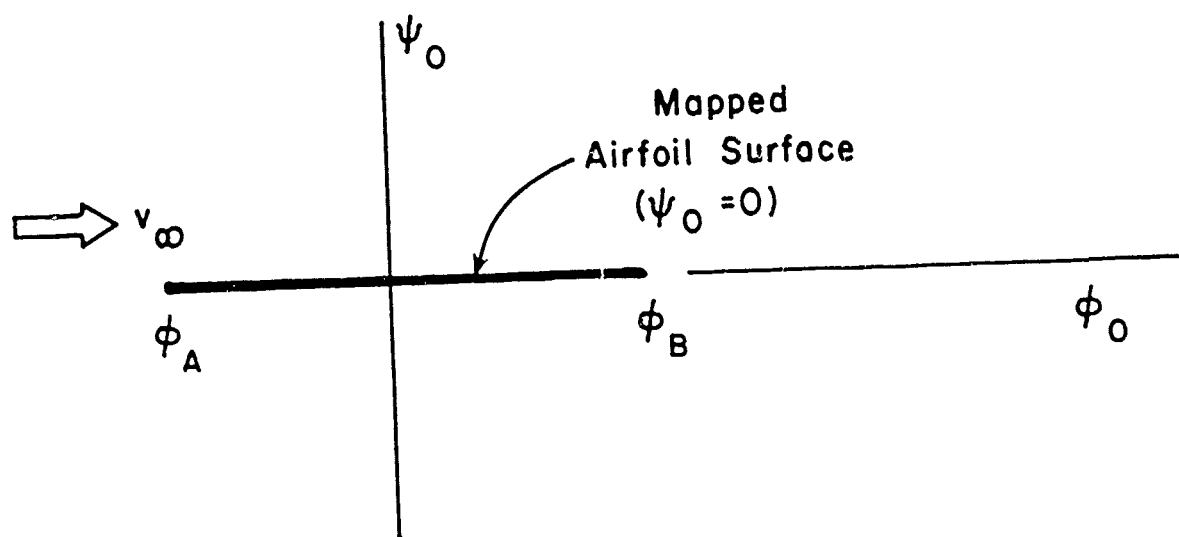The solution of Eq. (2.20) may be expressed in terms of potential doublets on the real axis; i.e.,

Figure 2.2. - Airfoil in thickness flow coordinate system (ϕ_0, ψ_0).

$$\phi' = -\frac{1}{2\pi} \int_{\phi_A}^{\infty} \Delta\phi(\phi_0') \frac{\partial}{\partial\psi_0} \ln\mathscr{R} \, d\phi_0' \qquad (2.25)$$

where

$$\mathscr{R} = \left[(\phi_0 - \phi_0')^2 + \psi_0^2\right]^{\frac{1}{2}} \qquad (2.26)$$

Now for $\psi_0 \neq 0$

$$\frac{\partial\phi'}{\partial\psi_0} = \frac{1}{2\pi} \int_{\phi_A}^{\infty} \Delta\phi(\phi_0') \frac{\partial^2}{\partial\phi_0^2} \ln\mathscr{R} \, d\phi_0' \qquad (2.27)$$

Substitute Eq. (2.24) into Eq. (2.27), interchange the order of integration and take the limit as $\psi_0 \to 0^{\pm}$. We obtain the following integral equation for the load distribution:

$$\frac{1}{2\pi} \fint_{\phi_A}^{\phi_B} \mathscr{L}(\phi_0') \, K(\phi_0 - \phi_0'; \phi_0') \, d\phi_0' = -\mathscr{W}(\phi_0) \qquad (2.28)$$

where

$$K(\phi_0;\phi_0') = \frac{\partial}{\partial\phi_0} \int_{0}^{\infty} ds \, \exp\left(-i\omega \int_{\phi_0'}^{\phi_0'+s} \frac{\partial\tau}{q_0^2}\right) \frac{\partial}{\partial\phi_0} \ln|\phi_0 - s|$$

$$(2.29)$$

and the slash through the integral indicates a Cauchy principle value. The inviscid integral equation (2.28) and kernel function $K(\phi_0;\phi_0')$ will play central roles in the theoretical development of viscous thin airfoil theory.

The non-uniqueness of the potential flow problem is readily apparent from the integral formulation. The kernel function (2.29) has a Cauchy singularity at $\phi_0 = 0$. It follows that the integral equation has an eigensolution [see Eq. (2.39)]. Some auxilliary condition must be specified if inviscid

13

potential theory alone is to be useful. The alternative is to develop a viscous theory or to derive an appropriate auxilliary condition from viscous theory. That is the primary objective of this report.

Even though the solution of the potential theory integral equation is not unique, the essential effects of geometric and boundary layer displacement thickness are explicitly brought out. First of all the upwash and the load distribution are modified by the local surface speed. The unknown load function $\mathscr{L}(\phi_0)$ is actually the pressure coefficient based on the "local" dynamic pressure. The most important effect of thickness on the unsteady problem is to induce the variable phase factor in the kernel function. The quantity

$$T = \int_{\phi_0'}^{\phi_0' + s} d\tau/q_0^2 \qquad (2.30)$$

is physically the time for a vortex disturbance to be convected from the load point on the airfoil surface to the point where the upwash is observed. For the flat plate airfoil, T is proportional to the distance between the load and upwash points since the local convection velocity is the constant free stream velocity. For a body with finite thickness the variable phase becomes an important factor in the calculation of the out of phase component of the load. Because of this factor, we also note that the kernel (2.29) is not translation invariant as it is for a flat plate. In the integral equation, the unsteady kernel $K(\phi_0 - \phi_0'; \phi_0')$ depends on the explicit location of the load, ϕ_0', as well as the difference, $\phi_0 - \phi_0'$, between the load and upwash points.

C. Zero Thickness Viscous Theory

We return now to the viscous perturbation problem of Section A. For zero thickness and simple harmonic motion the perturbation problem becomes

$$\text{div} \, \vec{v}' = 0$$

$$\frac{D_\infty \vec{v}'}{Dx} + \text{grad} \, h' = \nu \, \nabla^2 \vec{v}'$$

14

$$\left. \begin{array}{l} \vec{j} \cdot \vec{v}' = \dfrac{D_\infty f}{Dx} \\[3mm] \vec{i} \cdot \vec{v}' = 0 \end{array} \right\} \quad \begin{array}{l} \text{on} \quad y = 0^\pm \\[3mm] x_A < x < x_B \end{array}$$

$$|\vec{v}'| \sim 0 \qquad \text{at } \infty \qquad (2.31)$$

where

$$\frac{D_\infty}{Dx} = v_\infty \frac{\partial}{\partial x} + i\omega \qquad (2.32)$$

is the simple harmonic convective derivative. In a previous report (Ref. 2) an exact integral equation was derived for the zero thickness viscous problem. Here we express the kernel in the notation of Section B. With

$$q_0 = v_\infty , \qquad x = \phi_0/v_\infty , \qquad y = \psi_0/v_\infty \qquad (2.33)$$

the exact flat plate kernel function is

$$K(\phi_0) = \frac{\partial}{\partial \phi_0} \int_0^\infty d\phi_0' \; \exp\left(-\frac{i\omega \phi_0'}{q_0^2}\right)$$

$$\times \frac{\partial}{\partial \phi_0} \left[\ln|\phi_0 - \phi_0'| + \exp\left(\frac{\phi_0 - \phi_0'}{2\nu}\right) K_0\left(\frac{|\phi_0 - \phi_0'|}{2\nu^*}\right) \right]$$

$$(2.34)$$

where

$$\nu^* = \nu \left/ \left(1 + 2i\, \frac{\omega\nu}{v_\infty^2}\right)^{\frac{1}{2}} \right. \qquad (2.35)$$

15

and $K_0(z)$ is the modified Bessel function (Ref. 25). The solution of Eq. (2.28) with the flat plate viscous kernel, Eq. (2.34), was the subject of Ref. 2, where we also discussed the relationship of viscous thin airfoil theory to the theory of lift based on Oseen's equation (see Ref. 20). The main points are summarized below.

For any value of the viscosity, however small, the Cauchy singularity in the inviscid kernel is reduced to a symmetric logarithmic singularity as shown in Fig. 2.3. With a logarithmic singularity there are no eigensolutions of the integral equation (Ref. 26). The solution of the viscous flat plate airfoil equation is unique. As $\nu \rightarrow 0$ or Reynolds number Re tends to infinity, the solution tends to the potential flow result with the Kutta condition applied at the trailing edge. The results shown in Fig. 2.4 illustrate this point for the flat plate at constant angle of attack. For high Reynolds number, the difference between the viscous and inviscid solutions is of order $1/\sqrt{\text{Re}}$ except near the trailing edge, a result due to Shen and Crimi (Ref. 20). The calculated deviations from potential flow behavior near the trailing edge are not large enough to account for measured local deviations reported in Ref. 10. A summary of these detailed comparisons may be found in Ref. 2.

Far downstream, the effect of viscosity is to cause an exponential decay of the oscillating wake. For ordinary aerodynamic applications ($v_\infty \gg \sqrt{\omega \nu}$) the wake decay is of negligible importance and the complex kinematic viscosity ν^* in the kernel [see Eq. (2.35)] may be replaced by ν, thus simplifying the actual evaluation of the kernel. The direct effect of viscosity is quasi-steady.

Some additional features of the flat plate viscous theory (not reported in Ref. 2) can be brought out by comparing the integral formulation and solution for very low Reynolds number (Stokes flow) with the corresponding inviscid results. For simplicity consider the special case of steady flow over a flat plate airfoil at constant angle of attack, α. Introduce the dimensionless coordinate $x = 2\phi_0/v_\infty c$ where c is the airfoil chord. Then the low Reynolds number and infinite Reynolds number integral equations and solutions are respectively:

For $\sigma = v_\infty c/4\nu \rightarrow 0$ (Stokes Flow):

$$\frac{1}{2\pi} \int_{-1}^{1} \mathscr{S}(\xi) \left[\ln|x - \xi| + \ln \sigma + \gamma + 1 \right] d\xi = -\frac{\alpha}{\sigma}$$
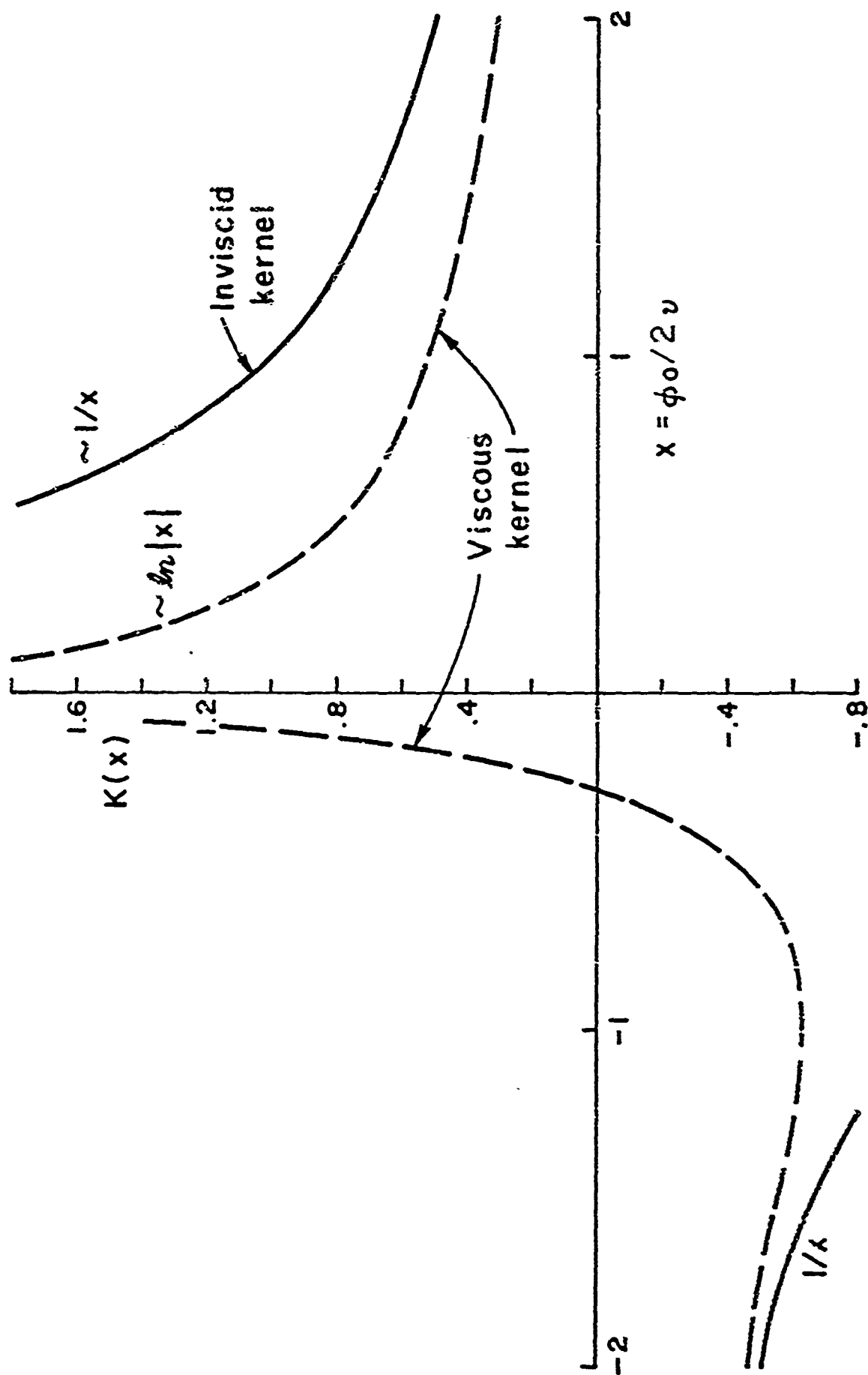
$$(2.36)$$

16

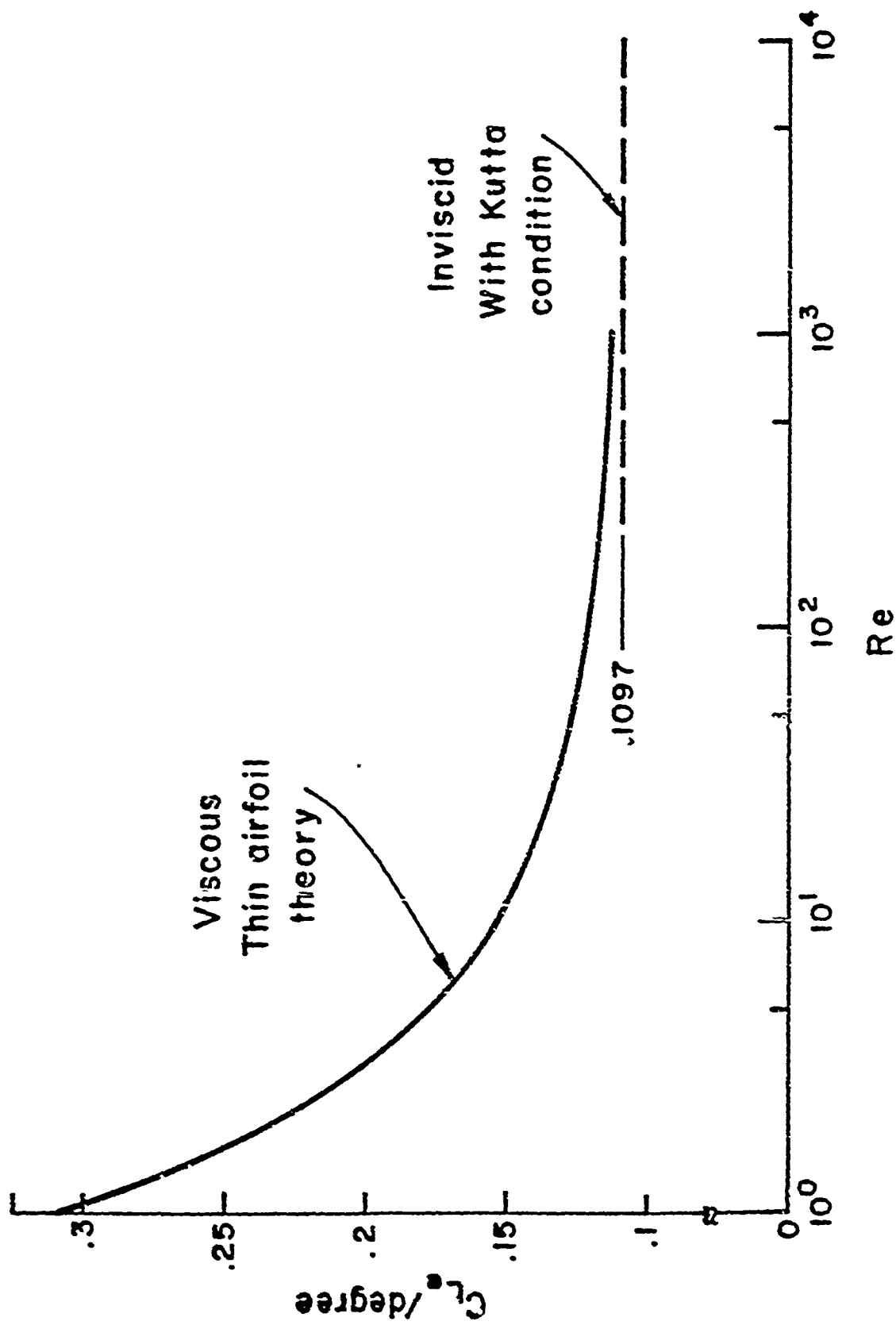Figure 2.3. - Kernel function of the steady viscous airfoil equation.

Figure 2.4. - Convergence of solution of the viscous airfoil equation for a flat plate at constant angle of attack.

where $\gamma \cong 0.57721$ is Euler's constant. The "unique"* solution is:

$$\mathscr{L}(x) = - \frac{\alpha}{\sigma \ln\frac{\sigma}{2} + \gamma + 1} \frac{1}{\sqrt{1 - x^2}} \qquad (2.37)$$

For $\sigma = \infty$ (Inviscid Theory):

$$\frac{1}{2\pi} \int_{-1}^{1} \frac{\mathscr{L}(\xi)}{x - \xi} d\xi = \alpha \qquad (2.38)$$

and

$$\mathscr{L}(x) = \frac{A}{\sqrt{1 - x}} - \frac{2\alpha x}{\sqrt{1 - x^2}} \qquad (2.39)$$

where A is an arbitrary constant, since $1/\sqrt{1 - x^2}$ is an eigensolution of Eq. (2.38).

The load distribution in the Stokes flow limit is precisely the same form as the "eigensolution" of inviscid theory. Although we have used high Reynolds number arguments to formulate the viscou thin airfoil problem there is nothing special about t..e formal application of the theory for low Reynolds number. In fact we expect a continuous dependence of the solution on Reynolds number. It follows that for a flat plate airfoil with mathematically sharp leading and trailing edges there must be a square root singularity at both edges, even though the flow is viscous. It is only at high Reynolds number that we see a tendency to weaken the trailing edge singularity. In this sense the mathematical statement of the Kutta condition is a limiting condition for high Reynolds number flow.

The most revealing feature of the foregoing comparison is that the ultimate origin of lift for any finite value of the Reynolds number is through the direct action of viscosity in

---

*For a general proof of uniqueness of Stokes flow see Batchelor (Ref. 18, p. 227).

the Stokes boundary layer. The eigensolution of so-called "inviscid" theory is actually the last remnant of the viscous effect, as it becomes more and more localized near the airfoil surface in the high Reynolds number limit. The auxilliary uniqueness statement (e.g., the Kutta condition, or principle of minimum singularity) that must be imposed on the family of potential flow solutions (see Section II.B, p. 9) is a statement about the "direct" effect of viscosity. The expression "inviscid" potential theory of lift is a misnomer since it is precisely the "singular" action of viscosity in the high Reynolds number limit that is ultimately responsible for the lift. This point was emphasized in a recent paper by Sears (Ref. 19).

D. Viscous Theory of Thin Airfoils

We now formulate the fundamental integral equation of viscous thin airfoil theory. The main result follows by comparison of the "exact" potential flow kernel that includes the effect of thickness [Eq. (2.29)] with the "exact" viscous flow kernel for the zero thickness airfoil [Eq. (2.34)]. The key observation is that for high Reynolds number and moderate reduced frequency the important viscous effect on the kernel is to reduce the order and modify the potential flow singularity over a distance of 0 $(c/\sqrt{Re})$ [see Eq. (2.34) and Fig. 2.2]. For $v_\infty \gg \sqrt{\omega\nu}$, a condition that is always satisfied in ordinary aerodynamic applications, the effect of viscosity is quasi-steady; i.e., $\nu^* = \nu$ in Eq. (2.35). Also the viscous effect is additive in the kernel [see Eq. (2.34)].

Now take the curl of the perturbation momentum equation (2.10) and transform into ϕ_0, ψ_0 coordinates. The result is

$$\nu \nabla^2 \Omega' - \left(\frac{\partial \Omega'}{\partial \phi_0} + \frac{i\omega}{q_0^2} \Omega' \right) = 0 \qquad (2.40)$$

where

$$\Omega' = \vec{k} \cdot \text{curl } \vec{v}' \qquad (2.41)$$

is the perturbation vorticity. Now let

$$\Omega' = \exp(\phi_0/2\nu) \, Q(\phi_0, \psi_0) \qquad (2.42)$$

Then

20

$$\nabla^2 Q - \frac{1}{4\nu^2}\left(1 + 4i\,\frac{\omega\nu}{q_0^2}\right)Q = 0 \qquad (2.43)$$

and for $q_0 \gg \sqrt{\omega\nu}$, the quasi-steady approximation, the fundamental solution of (2.43) is the modified Bessel function so that

$$\Omega' \cong \exp(\phi_0/2\nu)\, K_0(\mathscr{R}/2\nu) \qquad (2.44)$$

where

$$\mathscr{R} = (\phi_0^2 + \psi_0^2)^{\frac{1}{2}} \qquad (2.45)$$

The local "quasi-steady" viscous solution for a body with finite thickness is precisely of the same form in ϕ_0, ψ_0 coordinates as the corresponding flat plate expression (see Ref. 27). By analogy, the integral equation and kernel of viscous thin airfoil theory can be expressed as follows:

$$\frac{1}{2\pi}\int_{\phi_A}^{\phi_B} \mathscr{L}(\phi_0')\, K(\phi_0 - \phi_0';\, \phi_0')\, d\phi_0' = -\mathscr{W}(\phi_0) \qquad (2.46)$$

where

$$K(\phi_0;\, \phi_0') = \frac{\partial}{\partial\phi_0}\int_0^\infty ds\,\exp\left(-i\omega\int_{\phi_0'}^{\phi_0'+s} d\tau/q_0^2\right)$$

$$\times\; \frac{\partial}{\partial\phi_0}\left[\ln|\phi_0 - s| + \exp[(\phi_0 - s)/2\nu]\, K_0(|\phi_0 - s|/2\nu)\right]$$

$$(2.47)$$

The last two equations are the fundamental theoretical results of this report. Note that the kernel has a symmetric logarithmic singularity so that all of the integrals are to be interpreted in the ordinary sense. The weak singularity also implies that the solution of (2.46) is unique. Numerical calculations based on these equations are summarized in Section III.

III. NUMERICAL RESULTS

A. Method of Solution

To solve the integral equation (2.46) we first introduce the dimensionless variable

$$x = \frac{\phi_0}{2a\, v_\infty} \qquad (3.1)$$

where a is a length to be chosen such that

$$\phi_0 = \phi_A \qquad \text{when} \quad x = -1$$

$$\phi_0 = \phi_B \qquad \text{when} \quad x = 1 \qquad (3.2)$$

then the integral equation and kernel can be written in the dimensionless form

$$\frac{1}{2\pi} \int_{-1}^{1} \mathcal{L}(y)\, K(x-y;\, y)\, dy = -\mathcal{W}(x) \qquad (3.3)$$

where

$$K(x;\, y) = \frac{\partial}{\partial x}\, K_1(x;\, y) \qquad (3.4)$$

and

$$K_1(x;\, y) = \int_0^\infty d\xi \, \exp\left(-i\tilde{k} \int_y^{y+\tau} d\tau / Q_0^2 \right)$$

$$\times \frac{\partial}{\partial x}\left[\ln|x-\xi| + \exp[\tilde{\sigma}(x-\xi)]\, K_0(\tilde{\sigma}|x-\xi|) \right]$$

$$(3.5)$$

Also

22

$$Q_0^2 = q_0^2 / v_\infty^2$$

$$\tilde{k} = 2\omega \, a / v_\infty$$

$$\tilde{\sigma} = \frac{v_\infty \, a}{\nu}$$

$$\mathscr{L} = \left(\frac{\Delta p'}{\rho_\infty v_\infty^2}\right) \cdot \frac{1}{Q_0^2}$$

$$\mathscr{W} = \frac{\partial f}{\partial s} + \frac{i\tilde{k}}{Q_0} f \tag{3.6}$$

The last expression, the local dimensionless surface upwash, must be expressed in terms of the normalized potential coordinate, x. The parameter, s, is the distance along the airfoil surface. The variable x should not be confused with the streamwise Cartesian coordinate. We refer to $K_1(x; y)$ as the integrated kernel.

Next we expand the load function $\mathscr{L}(x)$ in a series of Chebyshev polynomials; i.e.,

$$\mathscr{L}(x) = \sum_{n=0}^{N} A_n \frac{T_n(x)}{\sqrt{1 - x^2}} \tag{3.7}$$

where $T_n(x)$ is the Chebyshev polynomial of the first kind (Ref. 25). Substitute (3.7) into (3.3), multiply by $\sqrt{1 - x^2} \, U_m(x)$ (Chebyshev polynomial of the second kind) and integrate from -1 to 1. The end result is a matrix equation for the unknown load coefficients, A_n; i.e.,

$$\sum_{n=0}^{N} C_{mn} A_n = g_m \qquad m = 0, 1, 2, \ldots, N \tag{3.8}$$

where

23

$$C_{mn} = \frac{(m+1)}{\pi^2} \int_{-1}^{1} \frac{T_n(y)}{\sqrt{1-y^2}}\, dy \int_{-1}^{1} \frac{T_{m+1}(x)}{\sqrt{1-x^2}}\, K_1(x-y; y)\, dx$$

(3.9)

and

$$g_m = -\frac{2}{\pi} \int_{-1}^{1} \sqrt{1-x^2}\; U_m(x)\, \mathscr{W}(x)\, dx \qquad (3.10)$$

If we compare the last three equations with the corresponding flat plate results [see Eqs. (5.2), (5.3) and (5.9) of Ref. 2] the main difference is that the unsteady integrated kernel in (3.9) is an explicit function of the load point as well as the difference between the load and upwash points - a direct consequence of the variable surface speed. It is a curious fact that the steady state kernel ($k = 0$), including thickness, is independent of the explicit load position. The spectral coefficients (3.9) of the integrated kernel are not only functions of the reduced frequency and Reynolds number, as in the flat plate case, but they are also functions of the cross-sectional geometry. The coefficients depend on the geometry both through the mapping functions (ϕ_0, ψ_0) and through the unsteady convective phase factor in the kernel. The actual numerical evaluation of the spectral coefficient is simplified with the trigonometric substitution

$$x = \cos\theta, \qquad y = \cos\phi \qquad (3.11)$$

in which case

$$C_{mn} = \frac{(m+1)}{\pi^2} \int_{0}^{\pi} \cos n\, \phi\, d\phi \int_{0}^{\pi} \cos[(m+1)\theta]\, d\theta$$

$$\times\ K_1(\cos\theta - \cos\phi;\ \cos\phi) \qquad (3.12)$$

The kernel is first evaluated for a discrete set of load points as a function of the difference argument. Then the C_{mn}'s

24

are evaluated by successive quadratures in the order indicated in Eq. (3.12). Since the integrated kernel K_1 is non-singular, the numerical integration poses no formal difficulty. The time consuming part of the operation is the detailed evaluation of the kernel.

B. The Kernel Function

It is a remarkable feature of two-dimensional viscous incompressible thin-airfoil theory that a kernel function for an oscillating airfoil with finite thickness can be derived, and furthermore, that in the mean flow coordinate system it has the same structure as the corresponding flat plate result. The steady flow induced by the geometric and boundary layer displacement thickness plays a most important role in the structure of the kernel.

In the remainder of this report we consider the thickness induced flow for the symmetric Joukowski family of airfoils. The complex thickness potential and mapping are given below.

$$\Phi_0 = v_\infty \left(w + \frac{a^2}{w} \right) \tag{3.13}$$

$$z = w - a\varepsilon + \frac{b^2}{w - a\varepsilon} = F(w) \tag{3.14}$$

On the surface of the airfoil

$$w = a\, e^{i\theta} \tag{3.15}$$

$$\Phi_0 = 2v_\infty a \cos\theta = \phi_0 + i\psi_0 \tag{3.16}$$

and

$$\frac{z_s}{a} = e^{i\theta} - \varepsilon + \frac{b^2/a^2}{e^{i\theta} - \varepsilon} \tag{3.17}$$

From (3.16) we see that the proper length scale in the dimensionless potential variable, x, in (3.1) is the radius of the airfoil circle in the w-plane. The parameters a, b are related to the airfoil chord, c, thickness ratio, τ^*, and eccentricity, ε, by the following formulae:

$$a = \frac{c}{4} \frac{1 + \tau^*}{\Sigma}$$

$$b = a \left(\frac{1 - \tau^*}{1 + \tau^*} \cdot \Sigma \right)^{\frac{1}{2}}$$

$$\Sigma = \frac{1 - \epsilon^4}{1 - \epsilon^2 \left(\frac{1 - \tau^*}{1 + \tau^*} \right)} \tag{3.18}$$

For the elliptic cross section $(\epsilon = 0)$, τ^* is the true thickness ratio. For $\epsilon \neq 0$, τ^* is slightly less than the true thickness ratio and is calculated with the thickness corresponding to the point $w = ia$ in the circle plane. The square of the speed on the stagnation stream line is given by [see Eq. (3.6)]:

$$Q_0^2 = \frac{|1 - a^2/w^2|^{\frac{1}{2}}}{|F'(w)|^{\frac{1}{2}}}$$

$$w = a e^{i\theta} \qquad 0 < \theta < \pi \quad \text{on the body}$$

$$w = a t \qquad 1 < t < \infty \quad \text{in the wake} \tag{3.19}$$

In the kernel, Eq. (3.5), we have,

$$x = \cos\theta, \qquad 0 < \theta < \pi$$

$$x = \tfrac{1}{2}(t + 1/t), \qquad 1 < t < \infty \tag{3.20}$$

and the dimensionless convective phase factor

$$\theta(x,y) = \int_x^y \frac{d\tau}{Q_0^2} \qquad \begin{array}{l} -1 < x < 1 \\ x < y < \infty \end{array} \tag{3.21}$$

26

Also note that the reduced frequency $\tilde{k}$ and Reynolds number $\tilde{\sigma}$ are based on the length scale a in the kernel. For the flat plate $a = c/4$, the reduced frequency scales with the semi-chord and the Reynolds number, Re, is referred to the full chord; i.e.,

$$k = \frac{\omega c}{2 v_\infty}$$

$$Re = \frac{v_\infty c}{\nu} \qquad (3.22)$$

Typical plots of Q_0^2 are given in Fig. 3.1a and b for the elliptic cross section ($\tau = 12\%$) and the Joukowski airfoil with cusped trailing edge ($\tau = 15\%$). The variable surface speed is integrated numerically to yield the typical convective phase factor illustrated in Fig. 3.2 [see Eq. (3.21)]. The results shown are for an elliptic cross section approximately 10% thick. The load point is at the leading edge and the vertical difference between the dashed and solid lines is proportional to the difference in convection times for a vortex disturbance moving over the elliptic surface versus the flat plate. The integration of the variable convective phase factor over the airfoil and the wake leads to significant unsteady effects in the actual kernel function. Typical plots of the kernel for a 15% thick elliptic airfoil with $k = 1$ and $Re = 500$ are shown in Figs. 3.3a, b and c for a load point at the leading edge, quarter chord and mid-chord. The variations of the kernel near the origin due to finite Reynolds number do not appear in a plot based on the scale of the airfoil chord. The viscous singular behavior is illustrated in the steady state kernel in Fig. 2.3. The dashed line in Fig. 3.3 is the kernel function for the flat plate. The difference between the flat plate and thickness kernel is significant, in particular near the trailing edge and in the wake. While these kernel variations are primarily due to finite thickness the actual steady and unsteady load distributions presented in the following section depend on interactive viscous and thickness effects in a complicated way that is not fully understood. The competing effects of viscosity and geometry are known experimentally (see Sections C and D, below) and it is one of the important triumphs of viscous thin airfoil theory that these effects can be calculated.

C. Steady State Results

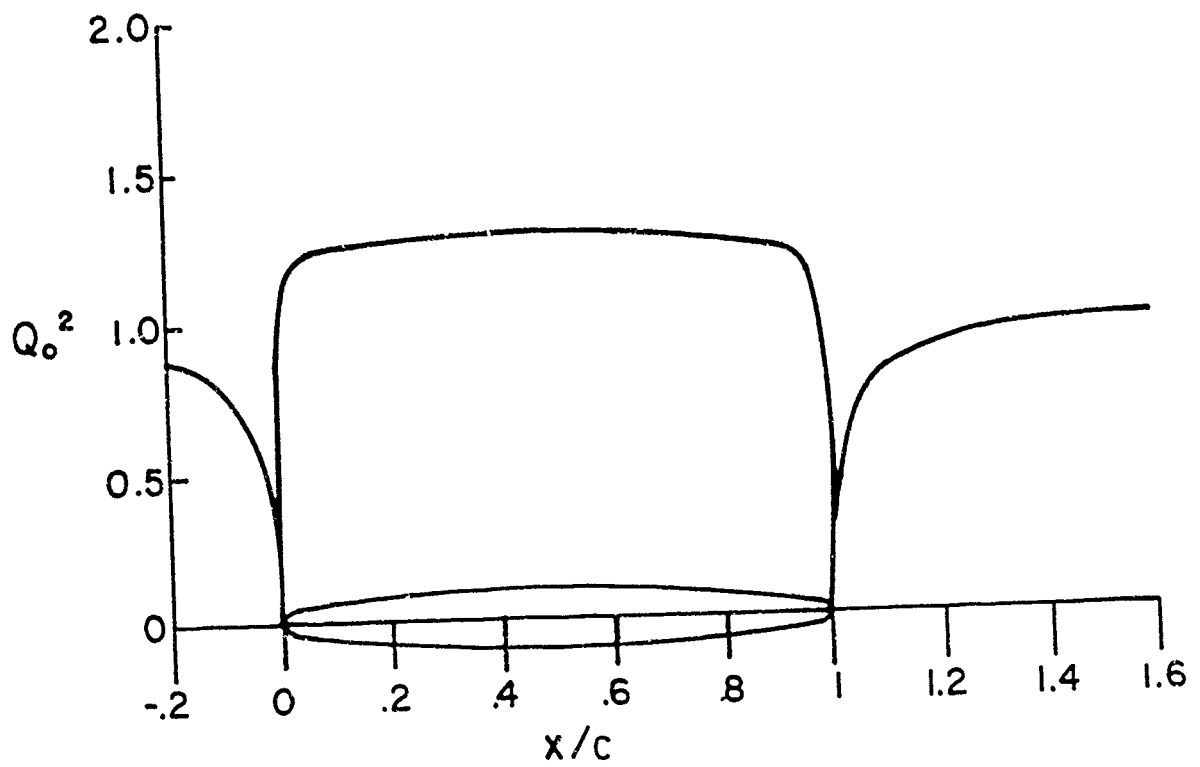The kernel function for the steady state problem is identical in form to the flat plate viscous kernel; i.e.,

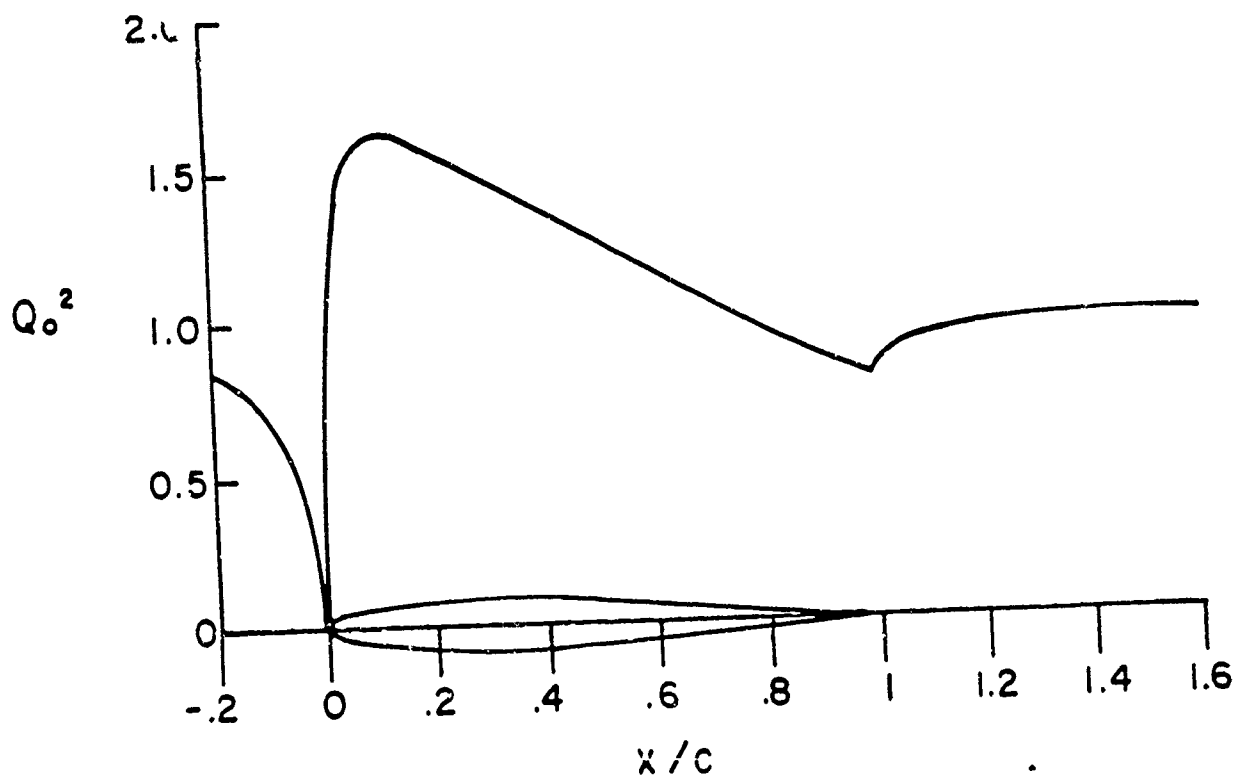Figure 3.1a. – Square of the surface speed on an elliptic
airfoil (τ = 12%).

28

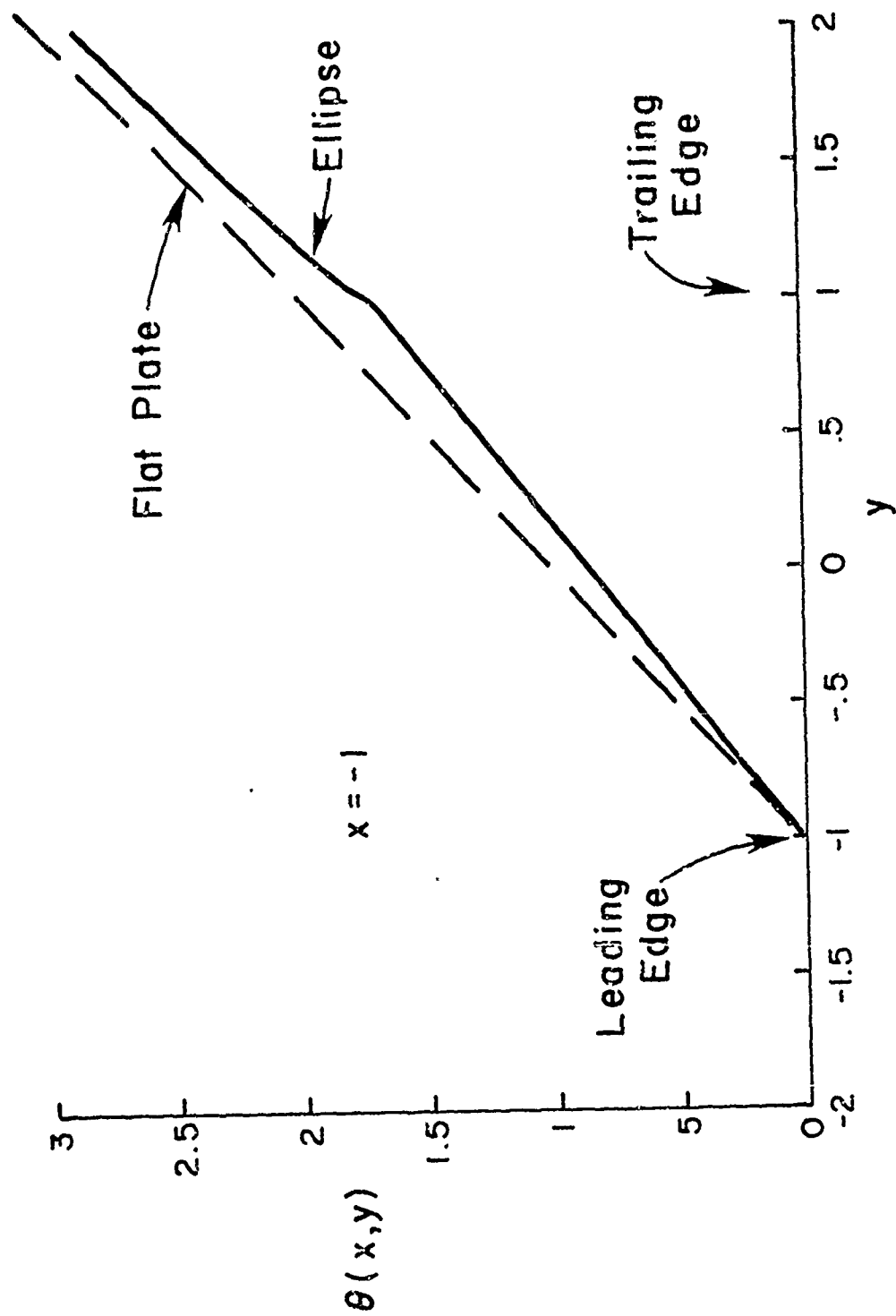Figure 3.1b. - Square of the surface speed on a Joukowski airfoil (τ = 15%).

29

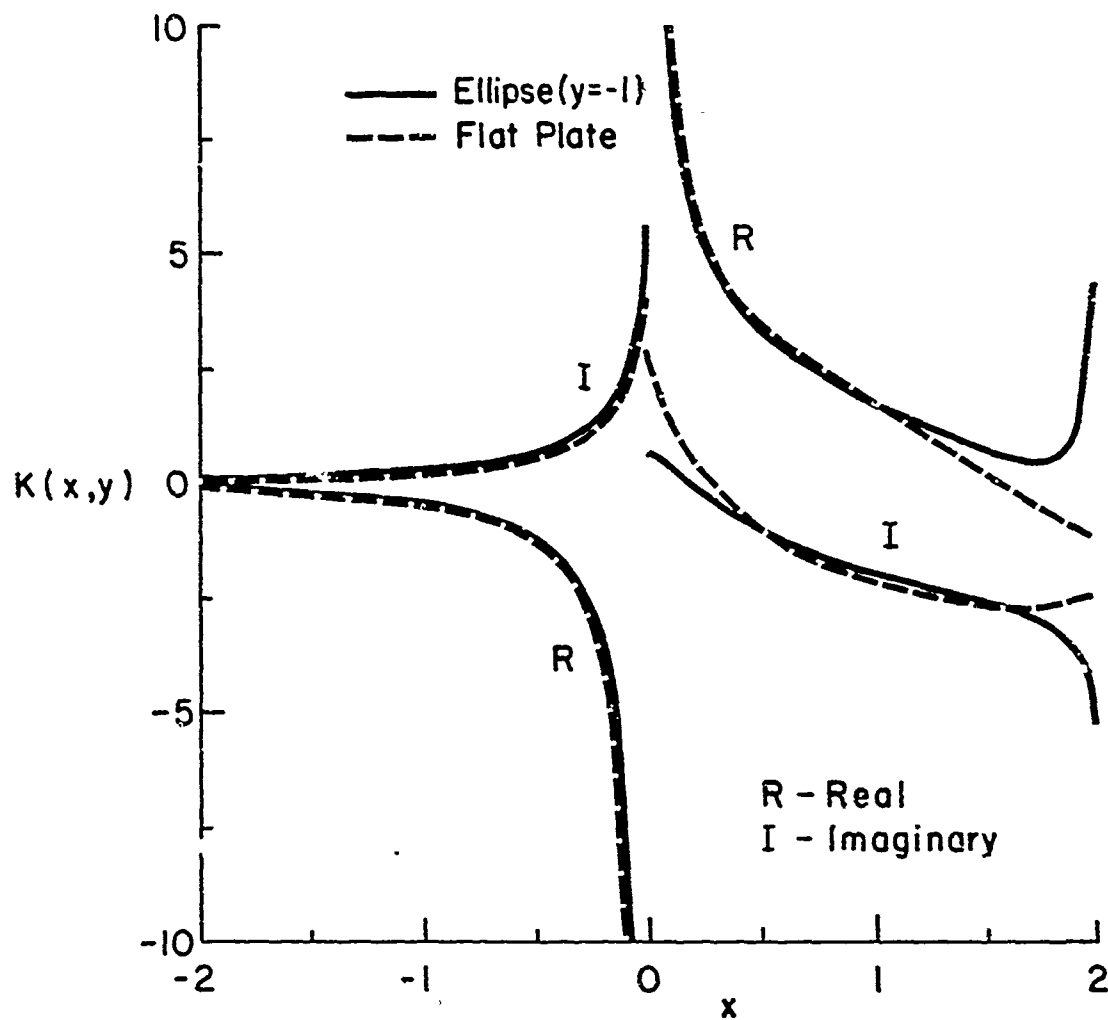Figure 3.2. - Typical convective phase factor (see Eq. 3.21) for an elliptic airfoil (τ = 10%).

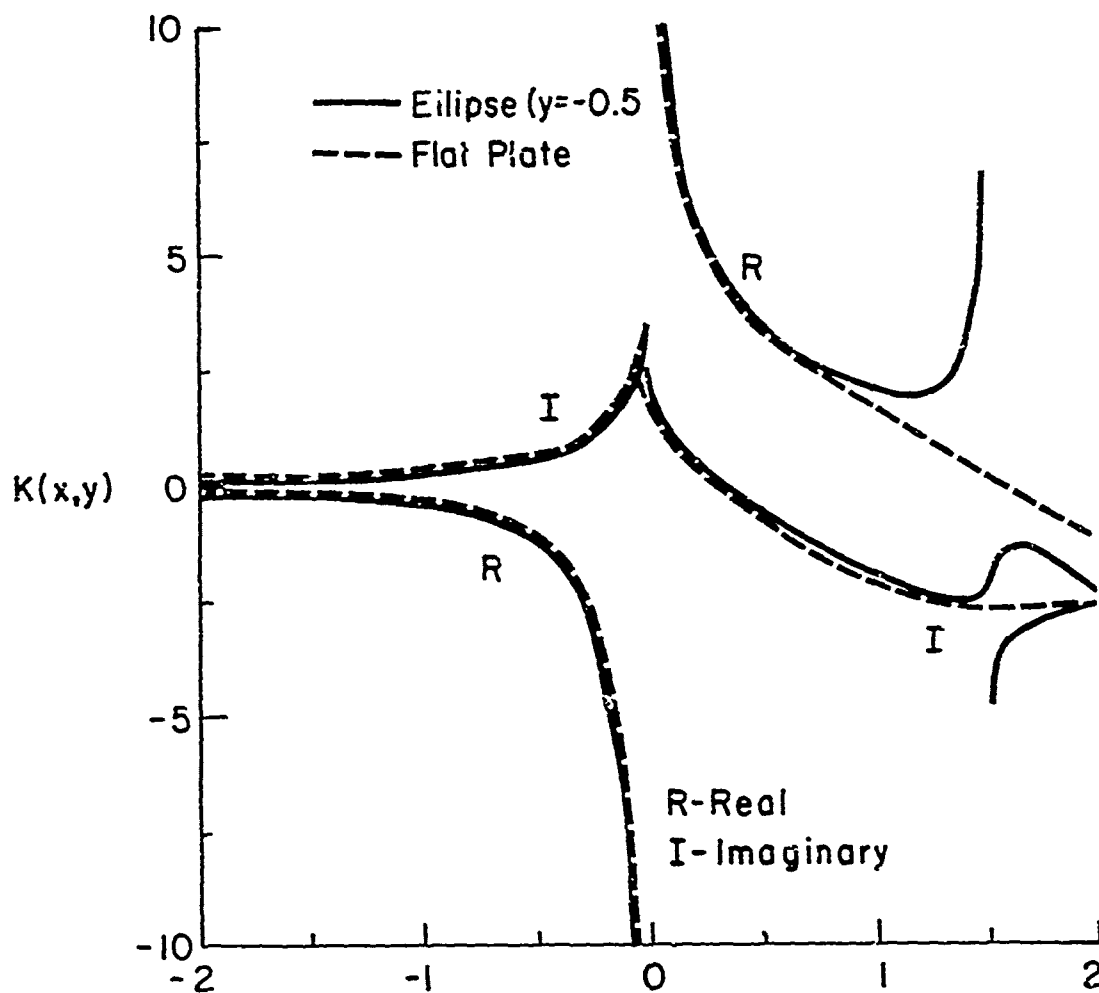Figure 3.3a. - Kernel function for elliptic airfoil (τ = 15%) for load point at the leading edge (y = -1).
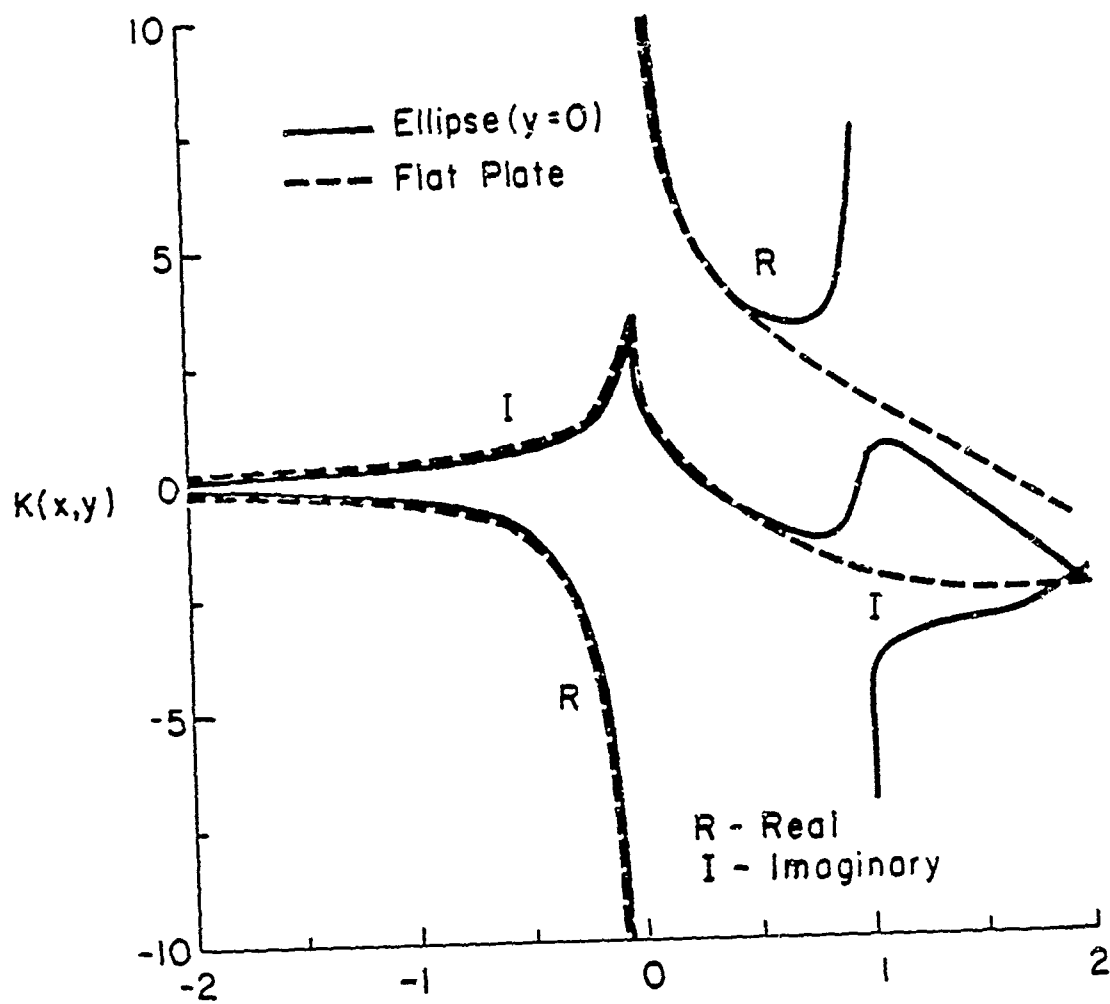
Figure 3.3b. – Load point at quarter chord (y = – 0.5).

32

Figure 3.3c. - Load point at mid-chord (y = 0).

33

(see Ref. 2)

$$K(x) = \frac{\partial}{\partial x} [\ln|x| + e^{\tilde{\sigma} x} K_0(\tilde{\sigma}|x|)] \qquad (3.23)$$

where x is the normalized potential coordinate and $\tilde{\sigma}$ is the Reynolds number based on the radius (approximately quarter chord) of the airfoil circle in the w-plane (see discussion in Section III.B). The load distribution on an airfoil with finite thickness can be expressed in terms of the corresponding flat plate solution in appropriate coordinates. From (3.6) we have

$$\frac{\Delta p'}{\rho_\infty V_\infty^2} = Q_0^2 \cdot \mathscr{L}(x) \qquad (3.24)$$

where $\mathscr{L}(x)$ satisfies the flat plate integral equation

$$\frac{1}{2\pi} \int_{-1}^{1} \mathscr{L}(y) K(x-y) \, dy = -\mathscr{W}(x) \qquad (3.25)$$

and

$$\mathscr{W}(x) = \frac{\partial f}{\partial s} \qquad (3.26)$$

is the modified upwash with thickness effects included. For a thin airfoil at constant angle of attack, α, we have

$$\mathscr{W}(x) = -\frac{\alpha}{1 + (h')^2} \qquad (3.27)$$

where h' is the local slope of the thickness distribution and must be expressed in terms of the potential coordinate x.

From our previous flat plate results we know that the solution of (3.25) has a square root singularity at the edges, although the trailing edge singularity is significantly weaker than the leading edge singularity for moderately large Reynolds numbers. It follows from (3.24) that the actual load distribution tends to zero for any edge that is.

34

not mathematically sharp (i.e., that does not have a cusp). This point is illustrated in Fig. 3.4a, b and c, where the lift distribution is given for a Joukowski airfoil with cusped trailing edge flying forward and backward, and for a near elliptic cross section. Note the tendency of the load distribution to become singular at the trailing edge in Fig. 3.4a. Because of the cusped edge the effect of viscosity is exaggerated and the overall lift and moment are overestimated.

The summary plots of the lift curve slope in Figs. 3.5 and 3.6 illustrate the competing effects of viscosity and geometry more clearly. Several important points concerning thickness are evident from Fig. 3.5. First we note the direct comparison of viscous and potential theory results for the standard Joukowski airfoil with cusped trailing edge. Except for differences of $0(1/\sqrt{Re})$ the results are the same. The increase in lift curve slope with increasing thickness predicted by potential theory with the Kutta condition is not realized in practice for actual airfoils. The experimental data shown in Fig. 3.5 are for the NACA 4 and 5 digit series airfoils (Ref. 17). The lift curve slope is less than the flat plate airfoil value and even decreases with increasing thickness ratio. For the NACA 63 through 66 series (Ref. 17, p. 130) there is a slight increase with thickness but the actual values are typically closer to the value predicted by flat plate thin airfoil theory (2π per radian or 0.1097 per degree). The competing effects of viscosity and geometric thickness lead to a nearly universal value for the lift curve slope on thin airfoils, that operate at high Reynolds number. This is probably the reason that flat plate airfoil theory has served the unsteady aerodynamicist so well.

The final curve in Fig. 3.5 is the lift curve slope for an elliptic airfoil section. The elliptic cross section is considered to be a reasonable model of an actual airfoil with the displacement thickness added on. The trend with thickness is very similar to the trend of the 4 and 5 digit series data. The actual levels are higher than should be calculated by a factor of $0(1/\sqrt{Re})$ (3 or 4% in the present calculations). Refinements could be introduced by an improved treatment of mean boundary layer effects. It must be emphasized, however, that the correct trend, due to geometric thickness, is calculated with only the inclusion of the "direct viscous effect" on a modified body shape (the elliptic section that emulates the thickness boundary layer). The improvement over the results of potential theory with the Kutta condition is significant.

Our final set of steady state results is shown in Fig. 3.6. The lift curve slope is plotted versus the modified eccentricity
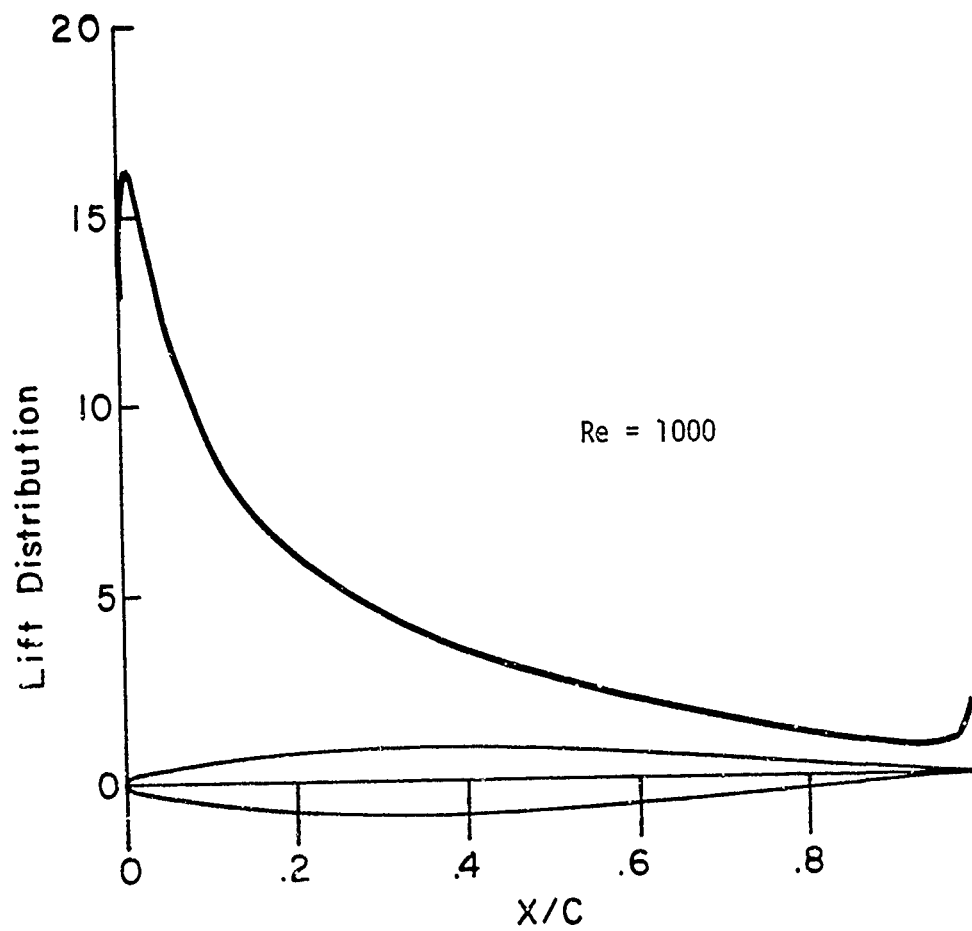
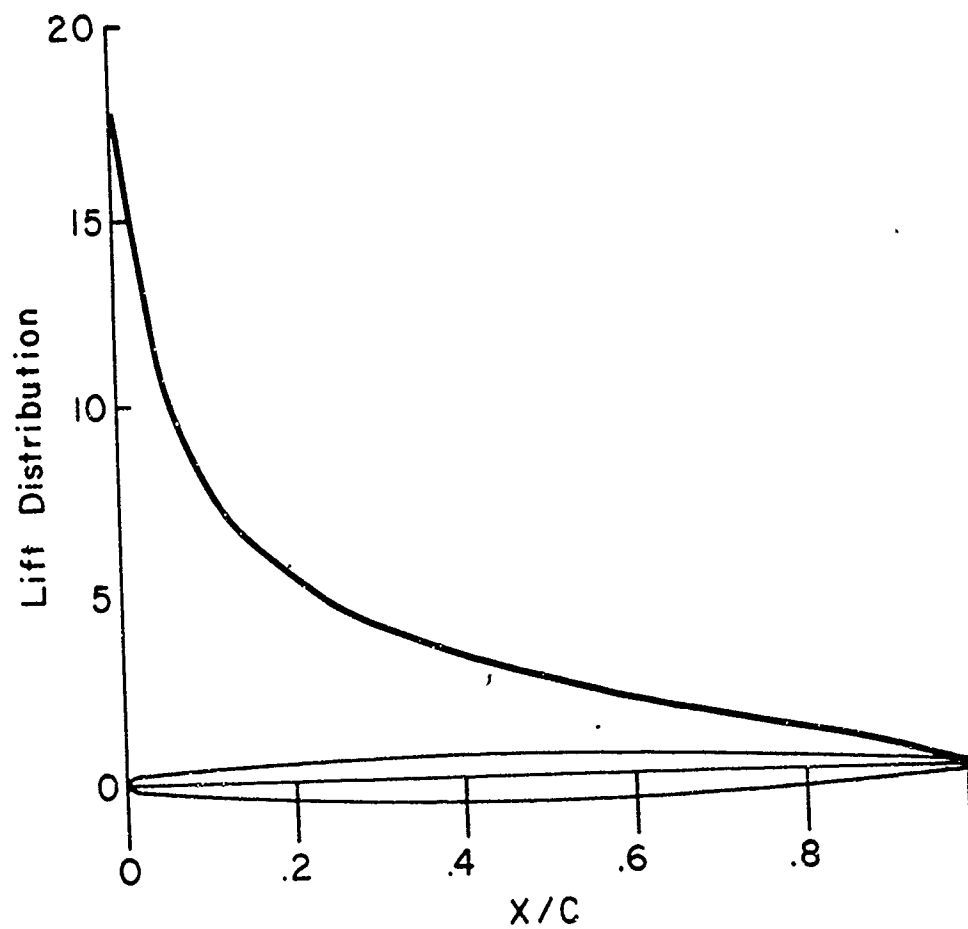Figure 3.4a. - Lift distribution for Joukowski airfoil flying forwards. $\tau = 14\%$.

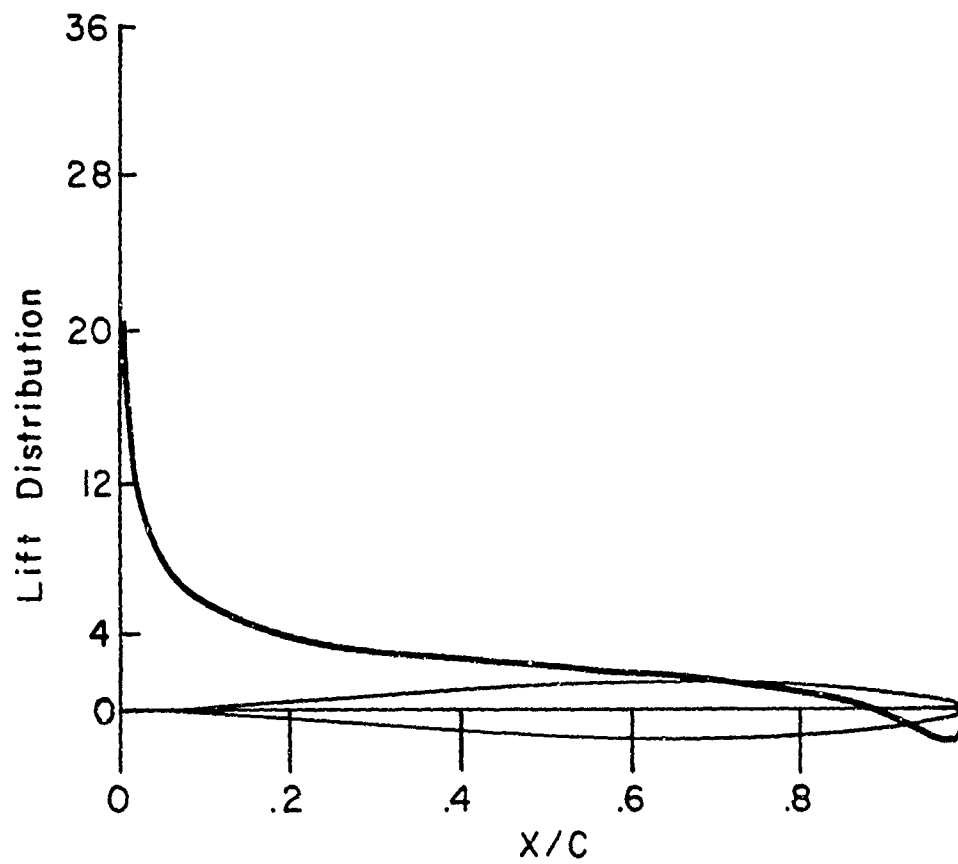Figure 3.4b. - Lift distribution for elliptic airfoil. $\tau = 12.5\%$.

Figure 3.4c. - Lift distribution for Joukowski airfoil flying
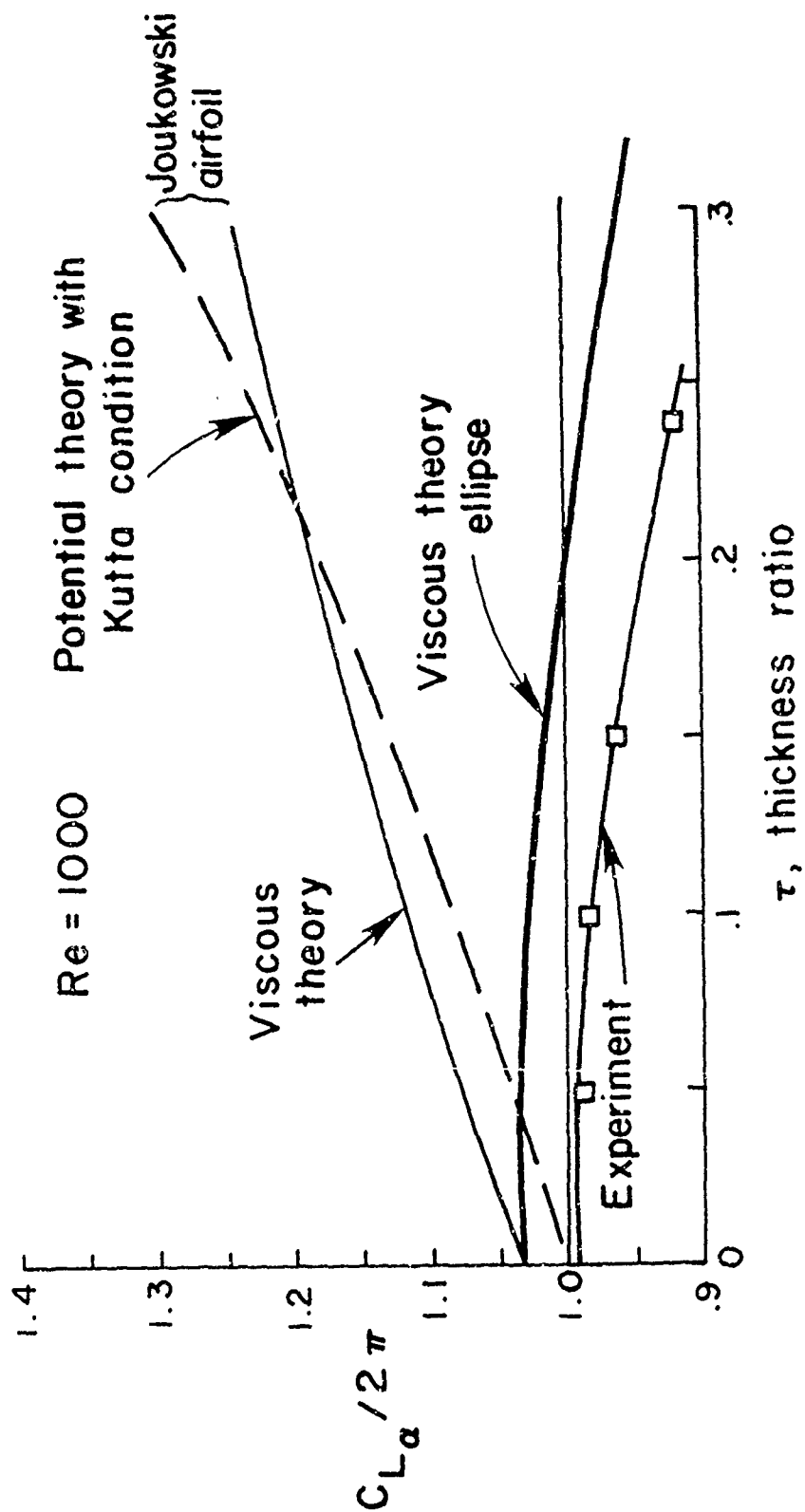backwards. τ = 14%.

Figure 3.5. - Lift curve slope versus thickness ratio. Comparison of theory and experimental results for the NACA 4 digit series airfoils (Ref. 17, p. 130).
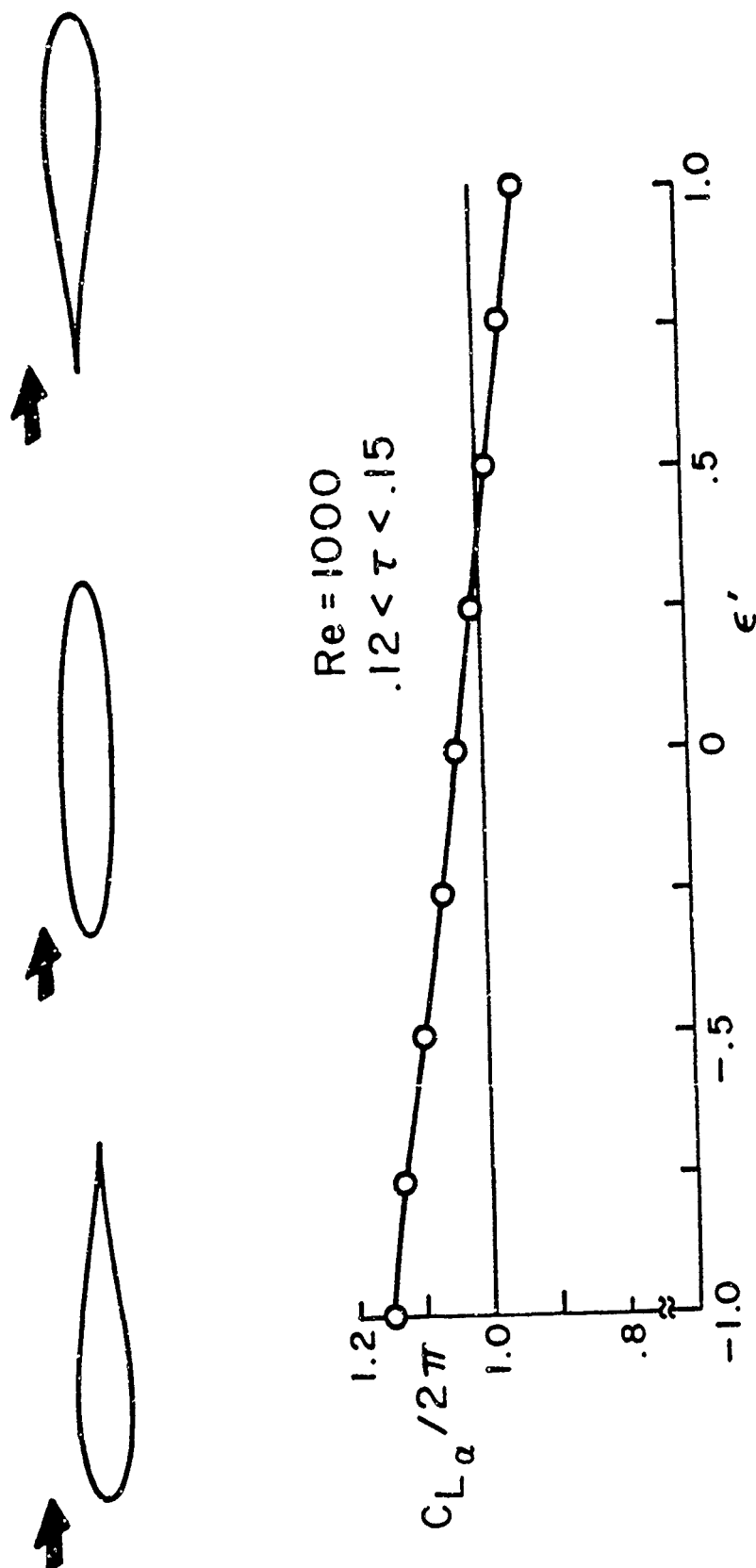
Figure 3.6. - Lift curve slope for the Joukowski family of airfoils.

40

parameter ε' that is linearly related to ε in the Joukowski mapping [see Eq. (3.17)] (i.e., $\varepsilon' = -\varepsilon/\varepsilon_{max}$). For $\varepsilon' = -1$, we obtain the conventional Joukowski airfoil with cusped trailing edge. For $\varepsilon' = +1$ the leading edge has a cusp and for $\varepsilon' = 0$ the section is elliptic. The trend of the calculated results is in approximate agreement with experimental data of Smith (Ref. 28) shown in Fig. 3.7. In particular, we call attention to the difference in lift curve slope for the cusped trailing edge and the elliptic section. The calculated reduction in C_{L_α} is 15% compared to a measured 20% reduction. Again the overall theoretical levels are higher than measured values for the cusped edge because of exaggerated viscous effects. The cusped leading edge airfoil has a further reduction in lift curve slope of about 10% from the elliptic section. The experimental data of Smith for a NACA 0012 section flying backwards is shown for comparison in Fig. 3.7. The cusped leading edge has a strong non-linear behavior for small angle of attack and it is difficult to infer a zero angle of attack slope. Our best estimate, indicated in Fig. 3.7 is about 50% of the value for the same airfoil flying forward. The theoretically calculated reduction in Fig. 3.6 is about 25%. It is interesting that for larger angles of attack the NACA 0012 flying forward and backward has a lift curve slope that is almost the same. The non-linear leading edge aerodynamics are beyond the scope of the linearized viscous thin airfoil theory.

D. Oscillating Airfoils - Comparison with Experiment

The calculations presented in this section are obtained by direct numerical solution of the complete integral equation of viscous thin airfoil theory [see Eq. (3.3)] with the kernel function defined by Eq. (3.5). The basic procedure is discussed in Section III.A. For the purpose of comparison with recent experimental data presented in Ref. 24, we consider the case of rigid body pitch. The unsteady downwash function [see Eq. (3.6)] for the pitching airfoil is:

$$ \mathcal{W} = -\left[\frac{1}{1 + (h')^2} + \frac{ik(\chi - \chi_0)}{Q_0[1 + (h')^2]^{\frac{1}{2}}} \right] \qquad (3.28) $$

where χ ranges from -1, at the leading edge, to $+1$ at the trailing edge. It is the normalized chordwise distance in the physical airfoil plane and like the local slope h', it is a function of the potential coordinate x through the mapping defined by Eqs. (3.16) and (3.17). The parameter χ_0 is the location of the pitch axis. For pitch about quarter chord
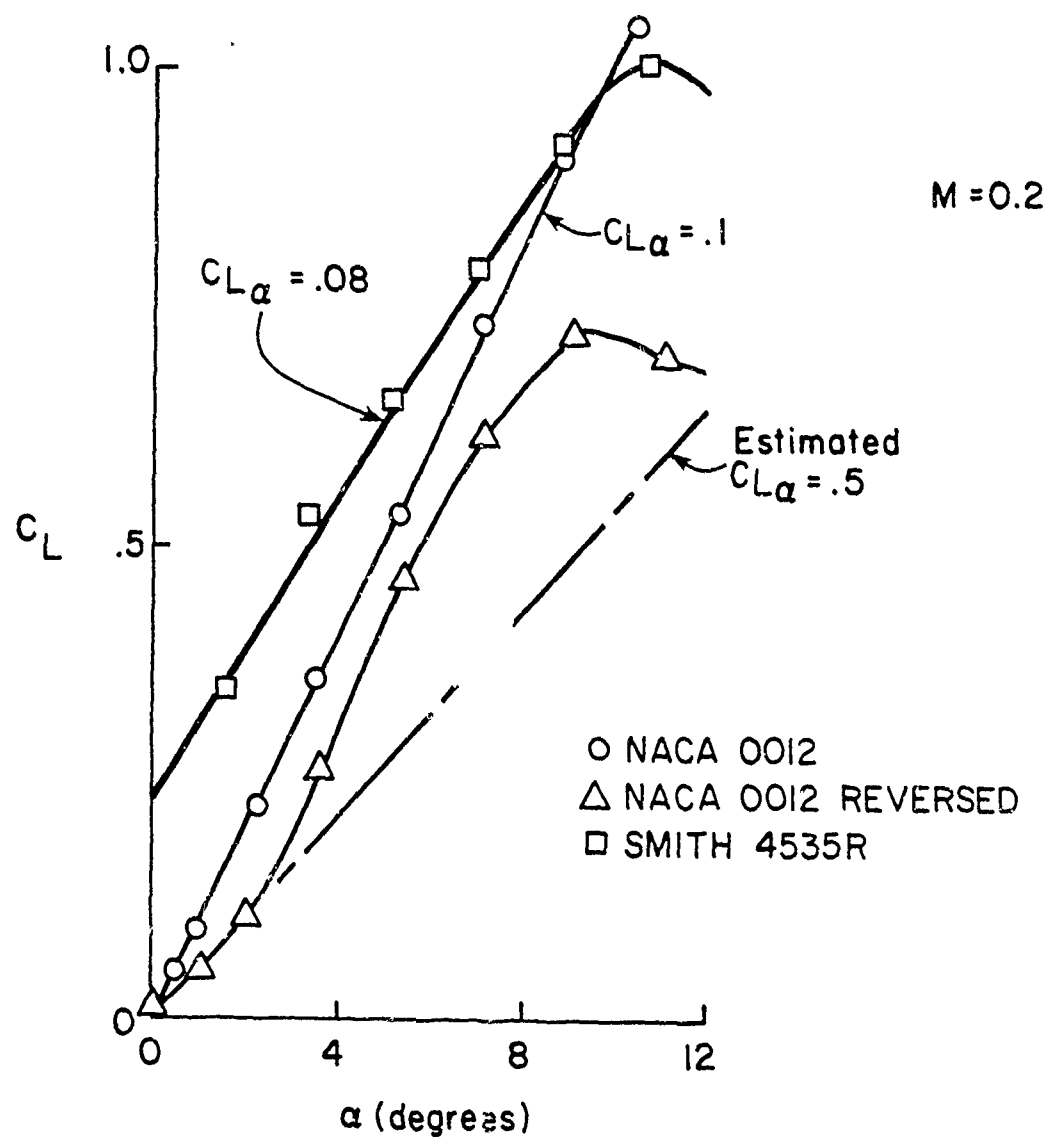
Figure 3.7. – Comparison of section characteristics of airfoils
Smith 4535R (Cambered Ellipse) and NACA 0012 (Ref. 28).

$X_0 = -0.5$. Calculations are presented for the elliptic airfoil and the Joukowski airfoil with cusped trailing edge ($\tau = 12\%$). Twenty-five Chebyshev polynomials are used to represent the load distribution and the computational Reynolds number is 500. Extensive calculations have shown that the numerical results are sensibly converged with errors of order $(1/\sqrt{Re})$. A typical steady state convergence plot for the flat plate airfoil is shown in Fig. 2.4, p. 18.

Typical chordwise load distributions for the elliptic airfoil and the Joukowski airfoil with cusped trailing edge are shown in Fig. 3.8a and b for a reduced frequency of 0.2. The pitch axis is at the quarter chord. These results may be compared qualitatively with the upper surface pressure measurements of Davis and Malcolm (Ref. 24) presented in Fig. 3.9. A direct quantitative comparison cannot be made because the Mach number is 0.5 in the experiment versus Mach zero in all of our calculations. However, there is a strong similarity between the measured and calculated results. The important point to note is the reduced loading on the elliptic cross section over the entire chord, in particular the out of phase load over the aft portion of the airfoil. The out of phase components of the overall lift and moment are quite sensitive to geometric shape, as we shall see below. We reiterate a point made previously that the elliptic cross section is considered to be more representative of the NACA 64A010 airfoil with boundary layer displacement thickness added on than the Joukowski airfoil with cusped trailing edge. The cusped edge is directly responsible for the exaggerated aft section loading in viscous thin airfoil theory. A direct application of the Kutta condition to potential theory leads to a similar exaggeration of the loads. Even though the experimental pressure (see Fig. 3.9) over the aft 20% of the airfoil chord is almost completely recovered, the application of the "least singular" condition on the potential flow pressure distribution at the trailing edge will lead to an overall estimation of the loads that is much too large. This point was most clearly brought out in the case of steady potential flow with Kutta condition for airfoils with finite thickness (see Fig. 3.5).

The most impressive display of unsteady calculations is presented in Fig. 3.10a, b, c and d, and should be compared with the corresponding experimental results presented in Fig. 3.11a, b, c, and d, from Ref. 24. The airfoil is oscillating about the quarter chord at reduced frequencies between zero and 0.3. The in-phase and out-of-phase components of the lift and the moment about the leading edge are plotted as a function of reduced frequency. Results are presented for the Joukowski airfoil with cusped trailing edge, the
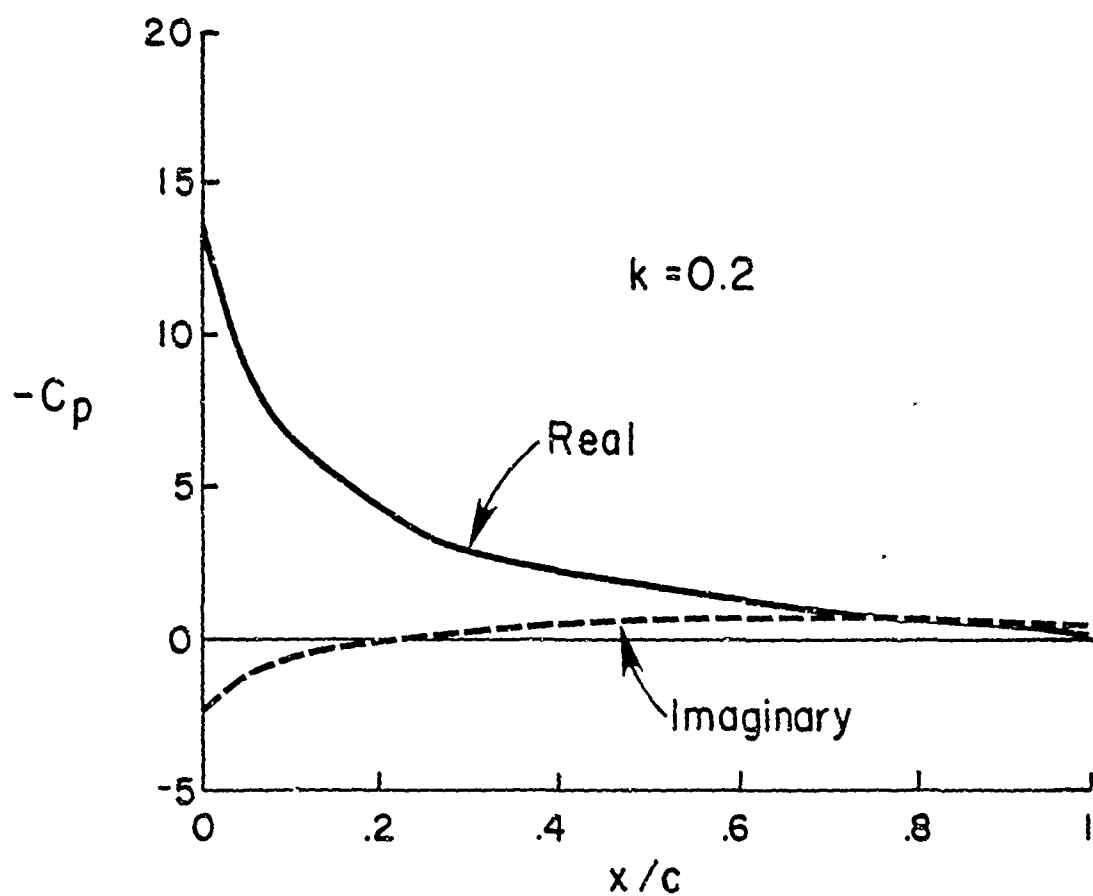
43

Figure 3.8a. - Upper-surface unsteady pressure distribution on a Joukowski airfoil with cusped trailing edge.
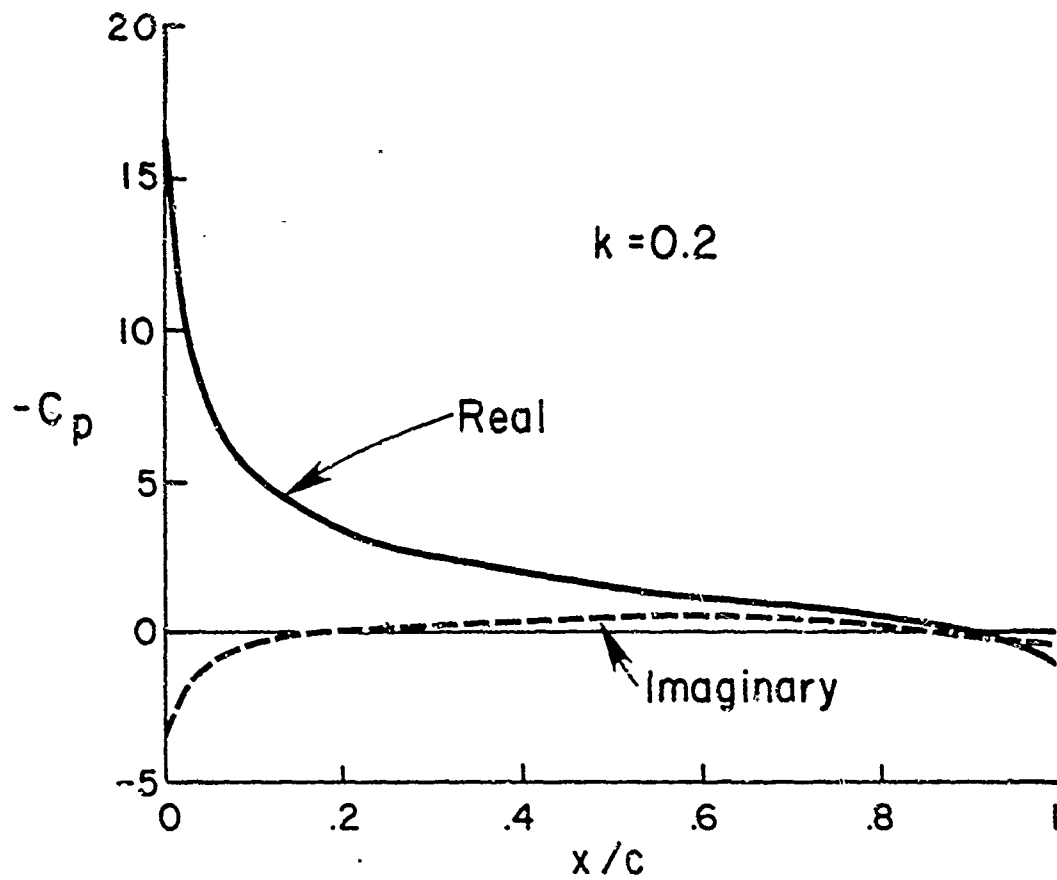
Figure 3.8b. - Upper-surface unsteady pressure distribution on an elliptic airfoil section.

PITCHING 1° @ 0.25C

M = 0.5
α_m = -0.13°
Re = 10 x 10⁶
k = 0.2
f = 22 Hz

O UPPER SURFACE, Re }
● UPPER SURFACE, Im } EXP.

LINEAR AERODYNAMICS
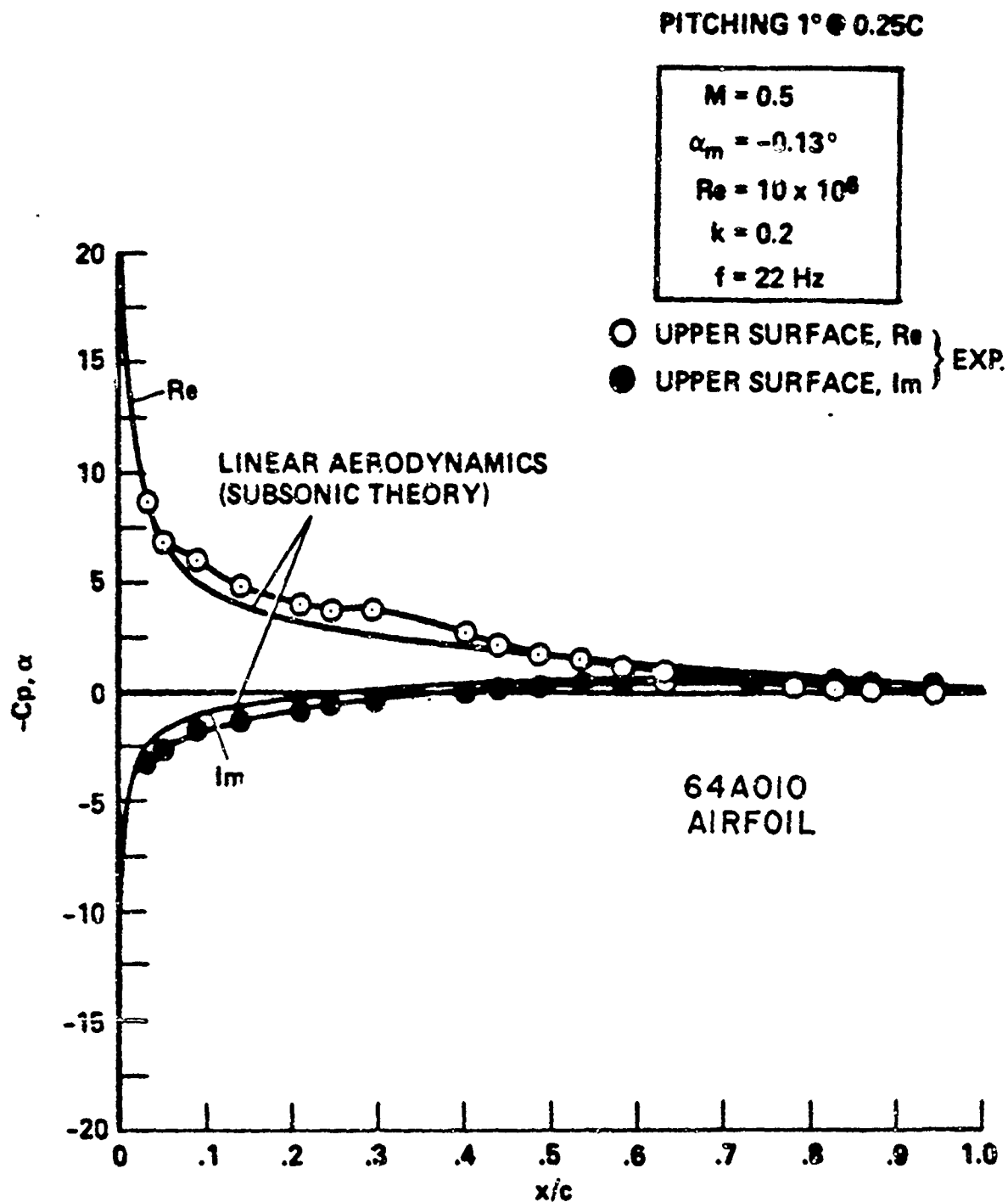(SUBSONIC THEORY)

64A010
AIRFOIL

Figure 3.9. - Upper-surface unsteady pressure distribution compared with
subsonic theory. (Ref. 10)
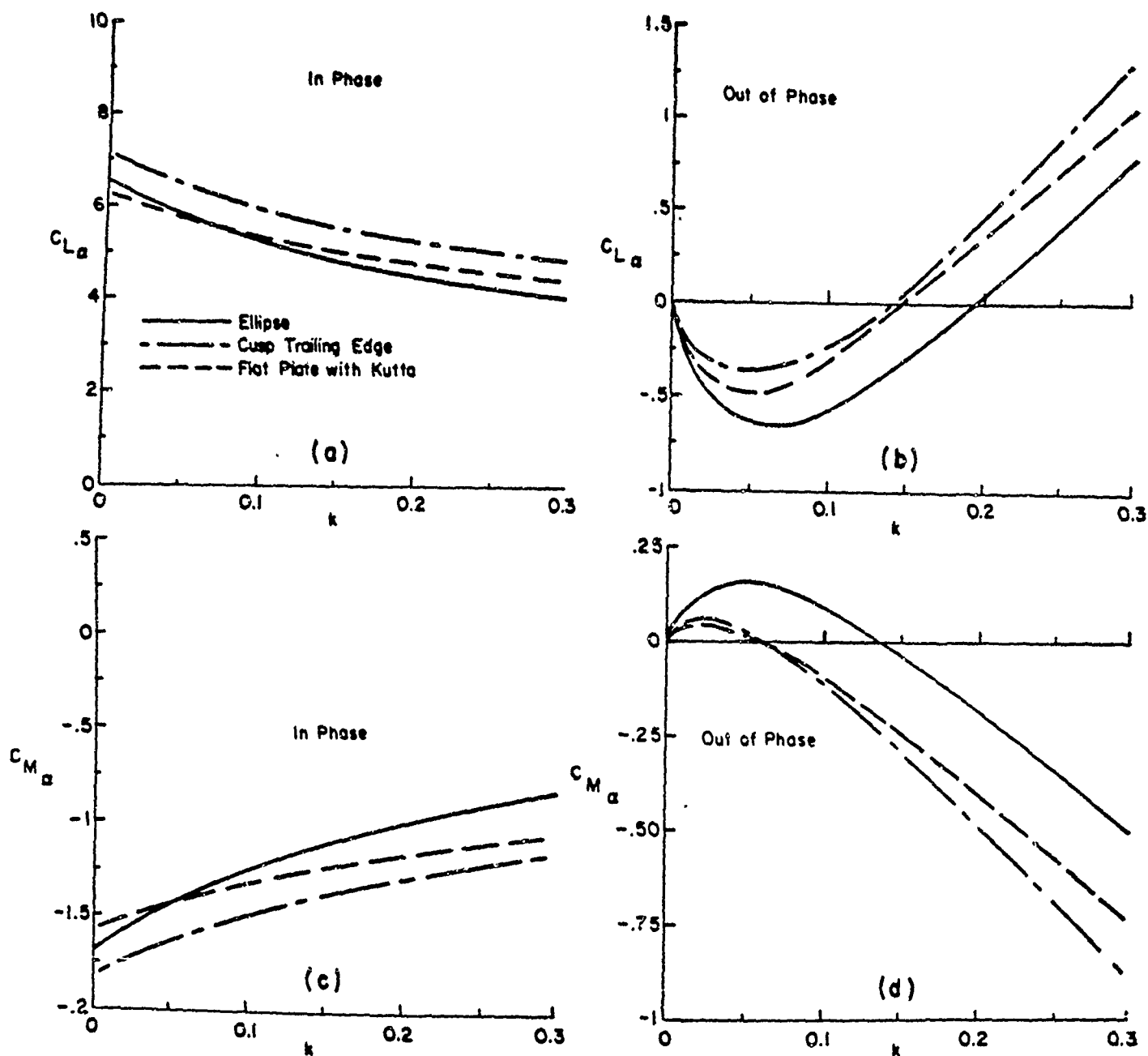
46

Figure 3.10. - Lift coefficient and moment coefficient (about the leading edge) versus reduced frequency; airfoil oscillating in pitch about the quarter chord.

AERODYNAMIC TRANSFER FUNCTION
SUBSONIC FLOW

PITCHING 1° @ 0.25C

$M = 0.5$
$\alpha_m = 0°$

○ Re = 10 x 10⁶
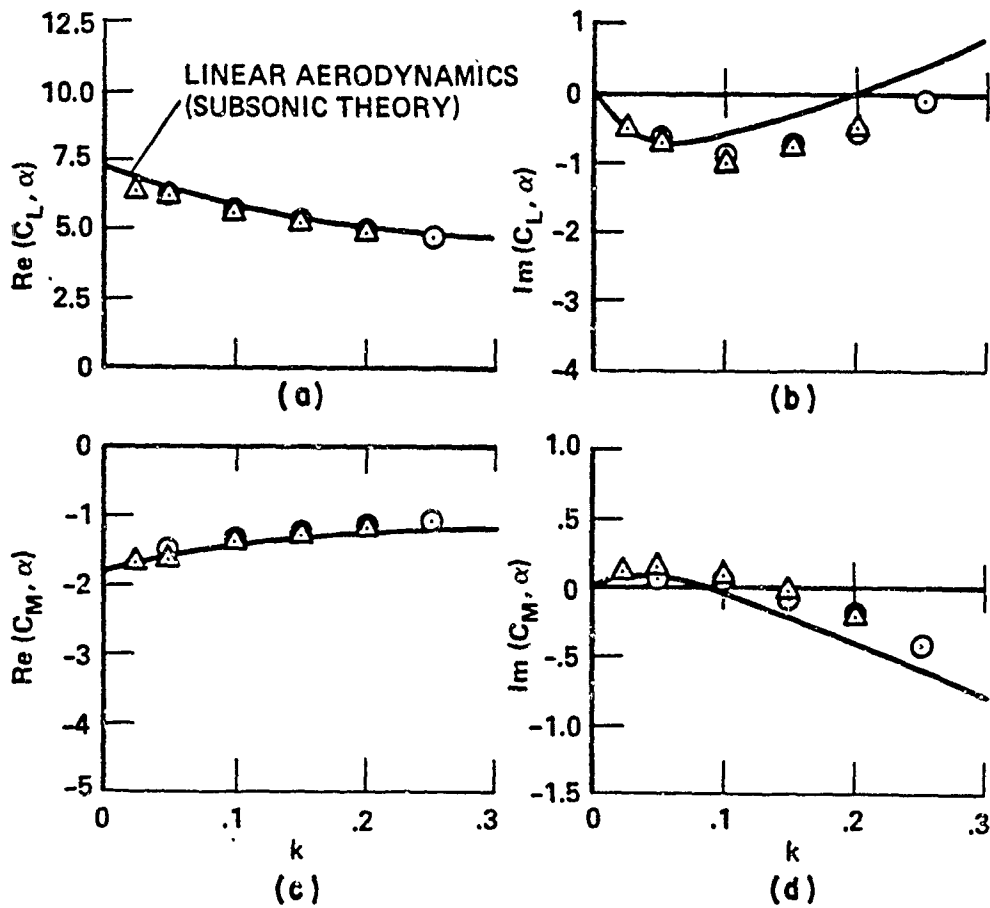△ Re ≈ 2.5 x 10⁶

64A0l0 AIRFOIL

Figure 3.11. - Experimental results for 64A010 airfoil. (Ref. 24)

elliptic cross section and the flat plate airfoil with
Kutta condition. The experimental results are for the NACA
64A010 airfoil at $M = 0.5$ and Reynolds number between
2.5 and 10 million. The theoretical curves shown in Fig. 3.11
were calculated in Ref. 24 by solving Possio's integral
equation.

The overall qualitative features of incompressible
viscous thin airfoil theory, inviscid thin airfoil theory
with Kutta condition and the experimental results at $M = 0.5$
are the same. Important quantitative differences are noted
upon closer examination. For example, the in-phase component
of the lift (Fig. 3.10a) on the elliptic section is about
15% less than the lift on the Joukowski airfoil. A similar
reduction in the magnitude of the leading edge moment is
noted in Fig. 3.10c. Note also that for reduced frequencies
greater than 0.05 the lift and moment on the ellipse are less
than the corresponding values for the flat plate airfoil with
Kutta condition. If we examine the experimental results
presented in Fig. 3.11a and c closely, we note first of all
that the symbols denoting experimental results are approxi-
mately 15% of the magnitude of the data plotted and further-
more that in each graph the theoretical curve tends to the
high side of the lift data and the low side of the moment
data. The reduction in the lift and moment that we have
calculated for the elliptic cross section are of the same
order of magnitude.

The out-of-phase components of the lift and moment are
plotted in Fig. 3.10b and d and should be compared with the
corresponding experimental and theoretical results in
Fig. 3.11b and d. In general the out-of-phase loading is
much more sensitive to geometry and reduced frequency than
the corresponding in-phase loading. The viscous thin airfoil
results for the cusped trailing edge are remarkably close to
the flat plate results. Such detailed comparison is
considered to be somewhat fortuitous. However, we note that
the elliptic section, that has a smaller positive loading
over the aft section (see Fig. 3.8a), has an overall lift
coefficient that is more negative and a smaller moment about
the leading edge. Also, in units of reduced frequency, the
zero crossing of the lift and moment for the elliptic section
is approximately 0.05 greater than the "sharp" trailing edge
results. A comparison of theory and experiment in Fig. 3.11b
and d reveals that the zero crossing of the experimental
results is also displaced to the right of flat plate (Possio)
theory by about 0.05 in units of k.

The improvement obtained in the out-of-phase component
of the lift and moment that we have calculated for the ellipse
is considered to be the most significant result, to date, of

viscous thin airfoil theory. We concur with the discussion by the authors of Ref. 24 that these global unsteady effects are in large measure due to non-uniform convection of disturbances. To the extent that the loading is primarily incompressible in origin the important phase lag is in the convection time for a vortex shed from a load point on the body to some point downstream. (Note the discussion of the phase factor in Section II.B, p. 14.) The vortex is in general accelerated over the body and retarded in the near wake. If compressibility is included in the theory, there will be additional phase lags due to differences in upstream and downstream propagation speeds.

IV. CONCLUSIONS AND RECOMMENDATIONS

The theory of incompressible two-dimensional viscous thin airfoils has been formulated in detail and numerical calculations have been presented for the symmetric Joukowski family of airfoil sections in steady flow and undergoing simple harmonic motion. Comparisons have been made with experimental data for steady and unsteady flow. The main conclusions of this work are summarized below:

1. Viscous thin airfoil theory can be reduced to the solution of an integral equation that is formally the same as the familiar equation of inviscid flat plate airfoil theory. The effect of viscosity is to reduce the order of the singularity in the kernel function and to establish a unique solution for airfoils of arbitrary cross section without an auxilliary uniqueness criterion such as the Kutta condition.

2. Steady flow viscous thin airfoil calculations for a cusped trailing edge airfoil with finite thickness are in agreement with the results of potential flow theory with Kutta condition. The calculated slope of the lift curve is much too large and has the wrong trend with increasing thickness ratio when compared with experimental data. Any practical attempt to include geometric thickness effects in steady or unsteady theory must account for the effective increased thickness of the aft section of the airfoil due to mean boundary layer displacement. With potential theory, the Kutta condition must at least be modified and with viscous thin airfoil theory an effective trailing edge bluntness must be accounted for.

50

3. The "direct" effect of viscosity 'n the
   Stokes layer over the entire airf !1 surface
   is the physical origin of circulatory lift
   for any Reynolds number.

4. The calculated out-of-phase loading on an
   oscillating elliptic airfoil is substantially
   different from the corresponding loading on
   a Joukowski airfoil with cusped trailing edge
   or the flat plate airfoil. The differences
   are due to a substantial reduction in the aft
   section loading and agree quantitatively with
   the differences between experimental data
   and direct solutions of Possio's integral
   equation at a Mach number of 0.5.

It is recommended that viscous thin airfoil theory be
extended in two directions of practical importance.

1. Incorporate viscous and geometric effects
   simultaneously in three-dimensional wing
   theory.

2. Incorporate viscous and geometric effects
   in Possio's integral equation for compressible
   flow and extend the theory towards the tran-
   sonic regime.

References

1. Yates, J. E.: Viscous Thin Airfoil Theory and the Kutta Condition. AIAA Paper No. 78-152, presented at AIAA Aerospace Sciences Meeting, Huntsville, Alabama, Jan. 16-18, 1978.

2. Yates, J. E.: Unsteady Viscous Thin Airfoil Theory. AGARD Report No. 671, Jan. 1979.

3. Yates, J. E.: A Brief Summary of Further Developments in Viscous Thin Airfoil Theory, A.R.A.P. Tech. Memo No. 79-5, Feb. 1979.

4. Morino, L.; et al.: Steady and Oscillatory Subsonic and Supersonic Aerodynamics Around Complex Configurations. AIAA J., Vol. 13, No. 3, Mar. 1975.

5. Morino, L.: A General Theory of Unsteady Compressible Potential Aerodynamics. NASA CR 2464, Dec. 1974.

6. Morino, L.; and Lee-Tzong Chen: Indicial Compressible Potential Aerodynamics Around Complex Aircraft Configurations. NASA SP 347, Part II. (in: Aerodynamic Analyses Requiring Advanced Computers, Mar. 1975).

7. Morino, L.: Steady, Oscillatory, and Unsteady Subsonic and Supersonic Aerodynamics. NASA CR 15-130, Production Version (SOUSSA - P1.1), Vol. 1: Theoretical Manual (to be published).

8. Smolka, Scott A.; Preuss, Robert D.; Tseng, Kadin; and Morino, Luigi: Steady, Oscillatory, and Unsteady Subsonic and Supersonic Aerodynamics. NASA CR 159131, Production Version (SOUSSA - P1.1), Vol. II: User Program Manual (to be published).

9. Geissler, W.: Nonlinear Unsteady Potential Flow Calculations for Three-Dimensional Oscillating Wings. AIAA J., Vol. 16, No. 11, Nov. 1978.

10. Satyanarayana, B.; and Davis, S.: Experimental Studies of Unsteady Trailing-Edge Conditions. AIAA J., Vol. 16, No. 2, Feb. 1978.

11. Gostelow, J. P.: Trailing Edge Flows over Turbomachine Blades and the Kutta-Joukowsky Condition. Gas Turbine Division of the American Society of Mechanical Engineers for presentation at the Gas Turbine Conf. and Products Show, Houston, Texas, Mar. 1975.

52

12. Yates, John E.; and Houbolt, John C.:   On the Aerodynamic
    Forces of Oscillating Two-Dimensional Lifting Surfaces.
    Aeronautical Research Associates of Princeton, Inc.,
    Princeton, N. J., A.R.A.P. Report No. 156, Dec. 1970.

13. Yates, E. Carson Jr.:   Modified-Strip-Analysis Method
    for Predicting Wing Flutter at Subsonic to Hypersonic
    Speeds.   J. of Aircraft, Vol. 3, No. 1, Jan.-Feb. 1966.

14. Woolston, D. S.; and Castile, G. E.:   Some Effects of
    Variations in Several Parameters Including Fluid
    Density on the Flutter Speed of Light Uniform Cantilever
    Wings.   NACA Tech. Note No. 2558, 1951.

15. Henry, C. J.:   Hydrofoil Flutter Phenomenon and Airfoil
    Flutter Theory.   IAS Paper No. 62-54, 1962.

16. Abramson, H. N.; Chu, W. H.; and Irick, J. T.:   Hydro-
    elasticity with Special Reference to Hydrofoil Craft.
    NSRDC Hydromechanics Lab, Research and Development
    Report No. 2557, Sept. 1967.

17. Abbott, I. H.; and Van Doenhoff, A. E.:   Theory of Wing
    Sections.   Dover Publications, Inc., New York, 1959
    (p. 62).

18. Batchelor, G. K.:   An Introduction to Fluid Dynamics.
    Cambridge University Press, 1967.

19. Sears, W. R.:   Unsteady Motion of Airfoils with Boundary-
    Layer Separation.   AIAA J., Vol. 14, No. 2, Feb. 1976.

20. Shen, S. F.; and Crimi, P.:   The Theory for an Oscillating
    Thin Airfoil as Derived from the Oseen Equations.   J.
    Fluid Mech., Vol. 23, part 3, 1965, pp. 585-609.

21. Brown, S. N.; and Stewartson, K. J.:   Trailing-Edge
    Stall.   J. Fluid Mech., Vol. 42, 1970, p. 561.

22. Daniels, P. G.:   On the Unsteady Kutta Condition.
    Q. J. Mech. Appl. Math, Vol. 31, part 1, 1978, pp. 49-75.

23. Melnik, R. E.:   Wake Curvature and Trailing Edge
    Interaction Effects in Viscous Flow Over Airfoils.
    ATAR Conference, March 7-9, 1978, Langley Research Center,
    Hampton, Virginia.

24. Davis, S. S.; and Malcolm, G. N.:   Experiments in Unsteady
    Transonic Flow.   AIAA paper No. 79-0769, presented at
    the AIAA/ASME/ASCE/AHS 20th Structures, Structural
    Dynamics and Materials Conference, St. Louis, Missouri,
    April 4-6, 1979.

25. Abramowitz, M.; and Stegun, I. A.; eds.: Handbook of Mathematical Functions (2nd Printing), National Bureau of Standards, Washington, D. C., 1964.

26. Carrier, G. F.; Krook, M.; and Pearson, C. E.: Functions of a Complex Variable Theory and Technique. McGraw-Hill, Inc., New York, 1966, Ch. 8.

27. Southwell, R. V.; and Squire, H. B.: A Modification of Oseen's Approximate Equation for the Motion in Two Dimensions of a Viscous Incompressible Fluid. Phil. Trans. of Roy. Soc., Series A, 232, 27 (1933).

28. Smith, R.: NASA Ames Research Center, private communication, Nov. 1979.

REPORT DOCUMENTATION PAGE		READ INSTRUCTIONS BEFORE COMPLETING FORM
1. REPORT NUMBER	2. GOVT ACCESSION NO.	3. RECIPIENT'S CATALOG NUMBER
4. TITLE (and Subtitle) Viscous Thin Airfoil Theory		5. TYPE OF REPORT & PERIOD COVERED Final Report - 1977 - 1980
		6. PERFORMING ORG. REPORT NUMBER A.R.A.P. Report No. 413
7. AUTHOR(s) John E. Yates		8. CONTRACT OR GRANT NUMBER(s) ONR-N00014-77-C-0616
9. PERFORMING ORGANIZATION NAME AND ADDRESS Aeronautical Research Associates of Princeton, Inc. 50 Washington Road, P.O. Box 2229 Princeton, New Jersey 08540		10. PROGRAM ELEMENT, PROJECT, TASK AREA & WORK UNIT NUMBERS
11. CONTROLLING OFFICE NAME AND ADDRESS Office of Naval Research 800 North Quincy Street Arlington, Virginia 22217		12. REPORT DATE
		13. NUMBER OF PAGES
14. MONITORING AGENCY NAME & ADDRESS(if different from Controlling Office)		15. SECURITY CLASS. (of this report)
		15a. DECLASSIFICATION DOWNGRADING SCHEDULE

16. DISTRIBUTION STATEMENT (of this Report)

17. DISTRIBUTION STATEMENT (of the abstract entered in Block 20, if different from Report)

18. SUPPLEMENTARY NOTES

19. KEY WORDS (Continue on reverse side if necessary and identify by block number)

20. ABSTRACT (Continue on reverse side if necessary and identify by block number)

The theory of oscillating thin airfoils in incompressible viscous flow is formulated (see Refs. 1, 2, 3 for earlier background material) and applied to the calculation of steady and unsteady loads on the family of symmetric Joukowski airfoils. The theory is reduced to the form of an integral equation with kernel function whose solution is obtained with a modal expansion technique familiar from flat plate thin airfoil theory. The effect of viscosity is to change the order of the singularity in the kernel function such that a unique solution is obtained for any cross sectional geometry without using an

DD $_{1\ JAN\ 73}^{FORM}$ 1473   EDITION OF 1 NOV 65 IS OBSOLETE

auxilliary uniqueness criteria like the Kutta condition or principle of minimum singularity. The principal unsteady effect related to thickness is to introduce an explicit phase factor in the kernel function that is proportional to the time for vortex disturbances to be convected from the load point to the upwash point.

Viscous thin airfoil calculations for an airfoil with sharp trailing edge are in agreement with the results of potential theory with Kutta condition. The overall steady loads calculated with either theory are in general much larger than measured values and have the wrong trend with increasing thickness ratio. The competing effects of thickness (both geometric and boundary layer displacement) and viscosity for an actual airfoil are such that the measured loads are in better agreement with flat plate theory than with the theoretical results for finite thickness airfoils with sharp trailing edges.

Viscous thin airfoil steady and unsteady calculations for an airfoil with elliptic cross section are in much better agreement with experimental results. The slope of the steady state lift curve decreases with increasing thickness ratio in agreement with the experimental trend. The out of phase loads calculated for an oscillating elliptic section are significantly different from either flat plate results or those for the Joukowski airfoil with sharp trailing edge. The magnitude of the difference is in quantitative agreement with the difference between calculations based on Poisso's integral equation and recent experimental data.

It is concluded that viscous thin airfoil theory is a practical tool for introducing simultaneously the effects of viscosity and geometric thickness in two-dimensional unsteady aerodynamic theory.